Geophys. J. Int. (2002) **150**, 1–17

Stress tensor inversions along the westernmost North Anatolian Fault Zone and its continuation into the North Aegean Sea

Anastasia A. Kiratzi

Department of Geophysics, Aristotle University of Thessaloniki, 54124 Thessaloniki, Greece. E-mail: Kiratzi@geo.auth.gr

Accepted 2002 April 17. Received 2002 April 4; in original form 2001 April 12

SUMMARY

Gephart & Forsyth's method has been applied to estimate stress orientations from earthquake fault-plane solutions of the westernmost North Anatolian Fault zone (NAFZ), its westward continuation in the Northern Aegean Sea, where it interacts with the normal faulting of central Greece, and of the western coastal parts of Anatolia. In total, 163 fault-plane solutions were used to invert for the stress tensor of 9 seismotectonic subregions. Magnitudes range from 1.1 to 7.4. All events have shallow focal depths; most occurred in the uppermost 15 km and very few in the 15 to 40 km depth range. The region studied is characterized by strike-slip (NAFZ), by transtension (Central Greece and western Anatolia) and by a strong signature of transpression in the Marmara area. From NAFZ to central Greece, the σ_3 axis changes, continuously and smoothly, its orientation from N35°E in the westernmost NAFZ to nearly North–South in continental central Greece, and the maximum horizontal stress, σ_{Hmax} changes from WNW–ESE to ~E–W. The total angle of lateral variation in the direction of either σ_{Hmax} or σ_3 is ~40°. In central western Anatolia the orientation of σ_3 is NNE–SSW (N10°E) while in southern western Anatolia it is NNW–SSE (N33°W). In both cases the development of the major grabens (Simav, Gediz, Menderes) is in agreement with the resolved stress tensor. At the termination of the NAFZ against central Greece the regime is complex. The dextral shear motion transferred from the east crosses the Pilion peninsula and northern Evia Island where it interacts with the major normal faults of continental Greece. These faults have variable orientations. The E–W trending Quaternary fault system and the NW–SE trending fault system, which is inherited from the past. The latter faults under the presently acting stress field are reactivated either as strike-slip faults with sinistral strike-slip component (when oriented at small angle in respect to σ_3) or as normal faults with small sinistral strike-slip component (when oriented at high angle in respect to σ_3). The occurrence of the recent 2001 July 26 Skyros event, which was clearly connected to a NNW–SSE fault with sinistral strike-slip motion, provides strong seismological evidence that the old structures can equally well be reactivated under the presently active stress field.

Key words: Anatolia, fault-plane solutions, Greece, stress tensor inversion.

1 INTRODUCTION

The Aegean Sea and the surrounding land areas (Fig. 1) have been considered a 'natural geophysical laboratory' due to the wide variety of tectonic processes encompassed. Plate motion models (DeMets *et al.* 1990) suggest that the Arabian and African plates move northwards relative to Eurasia at a rate of~25 mm yr^{-1} and 10 mm yr^{-1}, respectively. The northward movement of the Arabian plate causes the westward extrusion of the Anatolian plate (McKenzie 1970, 1972, 1978). Recent synthesis of geodetic data (Papazachos 1999; McCluskyet *al.* 2000) confirms the first order rigid behaviour of Anatolia and introduces a rigid Aegean plate. The relative motion between Anatolia and the Aegean plate is associated with significant internal deformation, expressed mainly as extension in the Aegean domain, as originally defined by McKenzie (1972, 1978).

The presence of two major strike-slip faults, the North Anatolian Fault (NAF) and the East Anatolian Fault (EAF), facilitates the westward motion of the Anatolian plate. The NAF is a dextral strike-slip fault (Fig. 1) that runs for about 1400 km from the Karliova triple junction in the east to the Aegean extensional regime in the west (McKenzie 1972, 1978; Dewey & Şengör 1979). Its western portion, as it enters into the Northern Aegean Sea splays into several branches; the two most pronounced are shown in Fig. 1. The northern branch is the most seismically active and its associated basins have depths of~1500 m. The southern branch is not as well developed and the associated basins are also not as deep. The

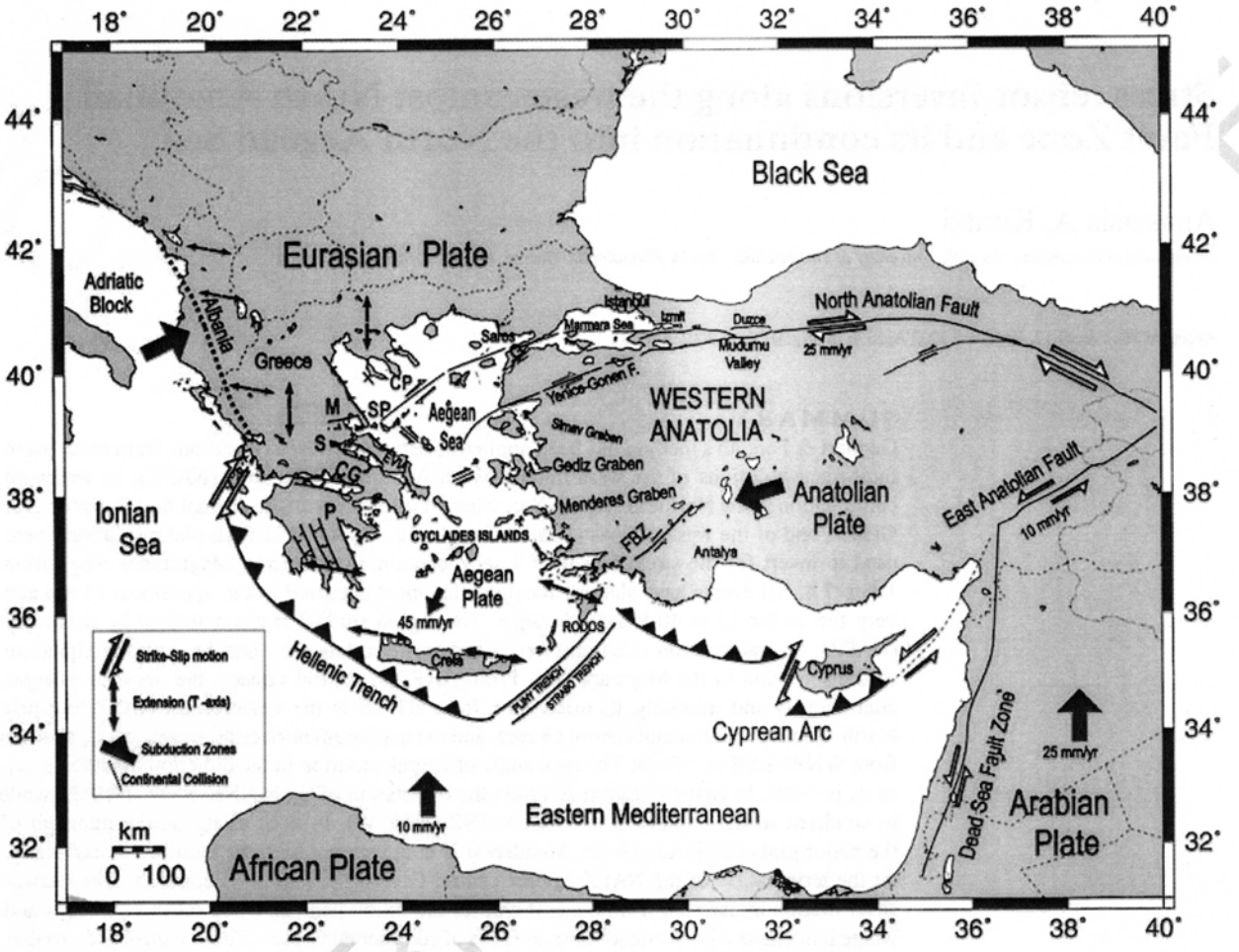

Figure 1. Simplified map of the Aegean Sea and the surrounding area. Solid lines are major strike-slip faults. Black arrows indicate the motion of the plates relative to Eurasia (McClusky *et al.* 2000). The small diverging black arrows indicate the direction of internal deformation (extension) in the broader Aegean area. (CG: Corinth Gulf; CP: Chalkidiki peninsula; FBZ: Fethiye-Burdur Fault Zone; G: Ganosdag; M: Magnesia basin; P: Peloponnese; S: Sperchios basin; SP: Sporades basin.)

branches of the NAF stop abruptly at the Sporades and Northern Evia Island basins and no-well defined structure has been recognised so far that is responsible for the transfer of the NAF motion to the Gulf of Evia and to the Gulf of Corinth. The Sporades and Evia basins are bounded, east of Pilion and east of Evia by NWSE striking faults, inherited from Pliocene times (Caputo 1990; Armijo *et al.* 1996). These old structures are morphologically dominant and are easily identified from topography and bathymetry (Lyberis 1984).

Stress tensor inversion has been applied here to a large set of focal mechanisms of the region that extends west of 32E and follows the northern boundary of the Aegean plate to the normal fault systems of central Greece (at 22°E) and in the transition zone between the Anatolian and the Aegean plate (Fig. 1). The main goal was to obtain the orientation of the principal stress axes and investigate the local stress field at a greater level of detail than previous studies. Other goals of this study were also: (a) to investigate the parameter resolution in the subregions for which earthquake focal mechanisms of variable magnitudes were simultaneously used (area of the interaction of the NAF with central Greece); (b) to investigate how accurately the inversion code chooses the fault plane from the two nodal planes and finally (c) to examine whether the orientation, slip vectors of these fault planes, (i.e. the failure planes with the smaller misfit), complimentary to other available information can shed light to the NAF zone-central Greece interaction.

Previous related work was performed by Bellier *et al.* (1997) for the region extending east of 32°E, by Zanchi & Angelier (1993), who used a different analysis method to resolve the regional stress in western Anatolia and by Cianetti *et al.* (1997) who used a Finite Element (FE) approach to model the deformation in the Aegean-Anatolian region.

2 STRESS TENSOR INVERSIONS

2.1 Method

The stress orientations were calculated following Gephart & Forsyth (1984) and Gephart (1990). Basic assumptions of the method are: (a) the deviatoric stress tensor is uniform within a region and over the time interval considered (b) earthquakes are shear dislocations on

pre-existing faults and (c) slip occurs in the direction of the resolved shear stress on the fault plane. The goal of the inversion is to find the stress state, which minimizes the discrepancy between the resolved shear stress direction and the slip direction for all earthquakes in the data set. Since only geometrical information is used the isotropic and deviatoric stress magnitudes cannot be estimated and there are only four independent model parameters. The algorithm inverts for the orientation of the three principal stress axes σ_1, σ_2, and σ_3 (maximum, intermediate and minimum compressive principal stress axis orientations, respectively, with magnitudes $\sigma_1 \geq \sigma_2 \geq \sigma_3$) and the parameter R $\{= (\sigma_2 - \sigma_1)/(\sigma_3 - \sigma_1);\ 0 < R < 1\}$. R is a scalar that describes the relative size of the intermediate principal stress σ_2 relative to the maximum σ_1 and minimum σ_3 compressive stresses.

The stress at a point (or at a volume of material in the case of homogeneous stress field over this volume) is generally classified according to the shape of the stress ellipsoid at that point. A triaxial stress state is a state in which all three principal stresses are nonzero, a biaxial stress state is a state in which only two principal stresses are nonzero and a uniaxial stress state is a state in which only one principal stress is nonzero. When σ_2 and σ_3 are nearly equivalent ($\sigma_1 > \sigma_2 \approx \sigma_3$), R approaches 1 (axial compression) and when σ_2 and σ_1 are nearly equivalent ($\sigma_1 \approx \sigma_2 > \sigma_3$), R approaches 0 (axial extension). These stress states require only minor fluctuations in stress magnitude to change from a strike-slip to a compressional regime ($0.85 < R < 1$), or from a strike-slip to an extensional regime (with $0 < R < 0.15$). The intermediate $R = 0.5$ ratio indicates a biaxial stress state for which $\sigma_2 = 0$. Between the near uniaxial ($0 < R < 0.15$ or $0.85 < R < 1$) and the near biaxial ($0.45 < R < 0.55$) stress states, the stress tensors characterize triaxial stress states. In this case, R-values higher than 0.55 indicate transpressional strike-slip regimes, in which σ_2 is tensional, whereas R-values lower than 0.45 indicate transtensional strike-slip regimes, in which σ_2 is compressional (Bellier *et al.* 1997).

The inversion scheme minimizes the differences between the slip direction, computed from trial stress tensors and the observed slip direction for both possible nodal planes for each focal mechanism. The difference between computed and observed slip direction is evaluated through an angular rotation (misfit), F, about an arbitrary axis. The misfit is the minimum angle that rotates the slip of one of the two nodal planes to match the resolved shear stress direction. This misfit is calculated through a grid search, systematically varying the orientation of the principal stresses and the parameter R. The stress tensor that corresponds to the minimum average rotation angle is assumed to be the best stress tensor for the specific population of focal mechanisms.

The minimum average misfit, F and the 95 or 90 per cent confidence limits of the best fitting model as described in Parker & McNutt (1980) and Gephart & Forsyth (1984) give an estimation of the homogeneity of the stressfield. In a series of tests for homogeneous stress cases, Wyss *et al.* (1992) found that errors in the data (focal mechanisms) of the order of 5°, 10°, and 15° were associated with misfit values not larger than 3°, 6°, and 8°, respectively.

In the commonly used inversion schemes the choice of the fault plane from the two nodal planes is important. Some of the earthquakes used here, produced surface breaks or well defined aftershock zones. In this case the choice of the fault plane was straightforward. In all other cases the fault plane was chosen by the inversion code and was that plane with the smaller angular misfit. Gephart & Forsyth (1984) suggest that this choice is optimal when the misfit, F, of the actual nodal plane is less than 20 and the misfit difference between the auxiliary plane and the fault plane is greater than 10°.

2.2 Data

After some initial test inversions and mainly based on the distribution of fault-plane solutions, the area was divided into 9 subregions. 163 focal mechanisms were used in total, which are listed in Table 1 and plotted in Figs 2(A) and (B). The shading variation of the beach balls indicates the different subregions studied. Magnitudes are in the range 1.1 to 7.4. To construct the database I first collected focal mechanisms determined by waveform modelling that were published in the literature. I then searched the Harvard CMT database to collect additional solutions; then I collected any first motion solutions available and finally I compiled the microearthquake focal mechanisms database. Most of the focal mechanisms used have been determined by waveform modelling. Microearthquake focal mechanism solutions were only available for the area near the termination of the NAF against central Greece and they have been all determined by first motion analysis (most of the events of Fig. 2b for instance are solutions published in Hatzfeld *et al.* 1999). It was assumed that all mechanisms were determined with errors in the strike, dip and rake of no more than 10°. All data were weighted equally, $w = 1$, with the exception of some large shocks, for which weight $w = 2$ was assigned (as noted in Table 1). With the small F values obtained through the inversion (see Table 2), and the assumed errors in the fault-plane solutions (~10°), I concluded that the stress homogeneity criterion is fulfilled in all cases. I did not attempt to invert for smaller subsets than the regions defined in Table 1 (or Fig. 2).

3 REGIONAL STRESS TENSORS

Table 2 summarizes the results of the inversions, which are described in the following for each region separately.

3.1 North Anatolian fault

Eleven focal mechanisms were used in the inversion (Fig. 2a). For 3 of those the fault planes were known *a priori*, since these events produced extensive surface ruptures. These events are the event of July 22, 1967 in Mudurnu Valley (Ambraseys & Zatopek 1969; Taymaz *et al.* 1991; Pinar *et al.* 1996), and the August 17, 1999 (Izmit) and November 12, 1999 (Düzce-Bolu) events (Bouchon *et al.* 2000; Yagi & Kikuchi 2000; Ayhan *et al.* 2001; Kiratzi & Louvari 2001; Tibi *et al.* 2001). In all three cases the E–W trending planes, exhibiting dextral strike-slip motion, were taken as the fault planes.

The computed stress tensor, as listed in Table 2 and shown in Fig. 3(a), shows pure strike-slip regime (σ_2 vertical). R equals 0.5, σ_{Hmax} trends ESE–WNW and σ_{Hmin} trends NE–SW. The minimum average misfit F is 3.3°.

3.2 Marmara

Twelve fault-plane solutions were used in the inversion (Fig. 2a). Few focal mechanisms are in the Marmara Sea itself, whereas most data cover the coast of Turkey. The geometry and the nature of the North Anatolian Fault under the Marmara Sea, from the Gulf of Izmit up to Ganosdağ has been a matter of debate. The recent work of LePichon *et al.* (2001) based on high resolution bathymetric data, indicates the existence of a single through going strike-slip fault system nearly bisecting the Marmara Trough that connects the 1999 Izmit earthquake fault with the 1912, Şaros-Gazikoy fault zone. However, the debate for the geometry of the continuation

Table 1. Earthquake data used, listed for each area separately. Shaded values of strike, dip and rake indicate known fault planes. Values of strike, dip and rake marked in bold italic letters indicate that these planes were the 'inferred' fault planes (see text from more information). Focal depths as reported in the corresponding references, an asterisk next to the value indicates that they were taken from Engdahl *et al.* (1998). Magnitudes, M are moment magnitudes in all cases except for the Hatzfeld *et al.* (1999) data, in which case they are coda magnitudes (regression against ML). An asterisk next to the magnitude indicates that the weight for the speci fic event was set equal to 2 during the regression.

Date	Origin time	Coordinates		Depth	M	Nodal plane 1			Nodal plane 2			P axis		T axis		Mo	Ref
yr/mo/dd	h/m/s	Lat. N	Long. E	(km)		Strike	Dip	Rake	Strike	Dip	Rake	Az	Pl	Az	Pl	*10e17 N m	
1. North Anatolian Fault																	
430620	15:32	40.70	30.38	10	6.5	86	90	166	176	76	0	132	10	40	10		McKenzie 1972
570526	6:33	40.50	31.25	10*	7.1	78	90	180	168	89	0	123	1	33	1	620.00	Jackson & McKenzie 1988
570526	9:36	40.60	31.30	10	6.0	78	90	180	168	89	0	123	1	33	1		Jackson McKenzie 1988
670722	16:56	40.67	30.69	12	7.2*	***275***	***88***	***−178***	185	88	−2	140	3	230	0	750.00	Taymaz *et al.* 1991
670730	1:31	40.70	30.40	16	5.6	***301***	***50***	***−110***	151	44	−67	146	74	45	3		McKenzie 1972
990817	0:01	40.81	30.08	11	7.4*	***266***	***85***	***−175***	176	85	−5	131	7	221	0	1150.00	Kiratzi & Louvari 2000
990831	8:10	40.79	29.94	15	5.1	82	78	−141	***342***	***52***	***−16***	309	36	207	17	0.47	Kiratzi & Louvari 2000
990913	11:55	40.42	30.24	16	5.7	***269***	***49***	***180***	360	89	41	127	27	233	28	4.90	Kiratzi & Louvari 2000
990929	0:13	40.55	29.69	15	5.2	66	48	−171	330	83	−42	279	34	25	23	0.69	Harvard CMT- solution
991111	14:41	40.95	30.10	13	5.6	297	55	−179	***206***	***89***	***−35***	156	25	257	23	2.64	Kiratzi & Louvari 2000
991112	16:57	40.93	31.25	12	7.1*	***262***	***53***	***−177***	170	88	−37	119	27	222	24	471.00	Kiratzi & Louvari 2000
2. Marmara																	
530318	19:06	40.02	27.25	7*	7.3*	60	90	180	150	89	0	105	1	15	1	870.00	Jackson & McKenzie 1988
641006	14:31	40.30	28.20	14	6.4*	100	40	−90	***280***	***50***	***−90***	190	85	10	5	41.00	Taymaz *et al.* 1991
690303	0:59	40.10	27.50	5	6.0	***60***	***40***	***68***	268	53	108	346	7	231	74	5.00	Taymaz *et al.* 1991
710223	19:41	39.60	27.37	15	5.4	***185***	***72***	***26***	86	65	160	314	5	47	31		Zanchi & Angelier 1993
720426	6:30	39.50	26.35	26	5.1	***150***	***73***	***−26***	248	65	−161	107	30	200	5		Zanchi & Angelier 1993
750327	5:15	40.34	26.14	15	6.2*	***68***	***55***	***−145***	316	62	−41	279	48	13	4	20.00	Taymaz *et al.* 1991
830705	12:01	40.32	27.22	10	6.1*	254	49	−173	159	85	−41	108	32	214	24	16.40	Harvard CMT- solution
831010	10:17	40.23	26.80	11	5.5	70	64	176	***162***	***86***	***26***	293	15	29	21	1.62	Louvari 2000
630918	16:58	40.80	29.10	15	6.4*	***304***	***56***	***−82***	110	35	−102	241	77	28	11	9.60	Taymaz *et al.* 1991
831021	20:34	40.09	29.33	15	5.4	217	90	180	***307***	***89***	***0***	262	1	172	1	1.64	Harvard CMT- solution
880424	20:49	40.83	28.24	15	5.3	355	70	−11	***89***	***80***	***−160***	313	21	221	7	1.04	Harvard CMT- solution
990819	15:17	40.68	29.10	15	5.1	***273***	***45***	***−120***	133	52	−63	105	69	204	4	0.63	Harvard CMT- solution
3. North Aegean Sea																	
490723	15:03	38.58	26.23	1	6.7	141	65	−30	***245***	***63***	***−152***	102	38	193	1		McKenzie 1972
640411	16:00	40.30	24.80	33	5.5	310	89	1	220	89	179	265	0	175	1		McKenzie 1972
651220	0:08	40.20	24.80	33	5.6	132	32	−90	312	58	−90	222	77	42	13		McKenzie 1972
670304	17:58	39.20	24.60	10	6.3	313	43	−56	***90***	***56***	***−118***	305	66	199	7	24.30	Taymaz *et al.* 1991
680219	22:45	39.40	24.90	10	7.0*	***216***	***81***	***173***	307	83	9	81	1	172	11	345.00	Kiratzi *et al.* 1991
811219	14:10	39.00	25.26	6	7.0*	***47***	***77***	***−167***	314	77	−13	271	19	181	0	224.00	Kiratzi *et al.* 1991
811227	17:39	38.90	24.90	6	6.4	***216***	***79***	***175***	307	85	11	81	4	172	11	38.20	Taymaz *et al.* 1991
811229	8:00	38.38	25.06	15	5.4	***330***	***63***	***10***	235	81	153	285	12	189	26	1.37	Harvard CMT- solution
820118	19:27	39.80	24.40	7	6.5*	***233***	***62***	***−173***	140	84	−28	93	24	190	15	73.20	Taymaz *et al.* 1991
830806	15:43	40.05	24.79	9	6.7*	***50***	***76***	***177***	141	87	14	275	8	6	12	121.00	Kiratzi *et al.* 1991
830826	12:52	40.46	23.96	15	5.2	***72***	***73***	***−168***	338	79	−17	294	20	26	4	0.64	Harvard CMT- solution
831010	10:17	40.23	25.32	11	5.5	70	64	176	162	86	26	293	15	29	21	1.62	Louvari 2000
840506	9:12	38.77	25.94	9	5.5	237	89	−161	147	71	−1	104	14	10	13	1.79	Louvari 2000
840617	7:48	38.86	25.72	15	5.1	156	73	−9	***249***	***81***	***−163***	113	19	22	6	0.62	Harvard CMT- solution
860325	1:41	38.34	25.19	6	5.6	163	59	−22	***265***	***71***	***−147***	127	36	32	8	2.55	Louvari 2000
860329	18:36	38.37	25.17	14	5.4	52	77	152	***149***	***63***	***15***	103	9	8	29	1.25	Louvari 2000
920723	20:12	39.81	24.40	8	5.4	272	51	−148	161	66	−43	120	47	220	9	1.13	Louvari 2000
971114	21:38	38.81	25.86	10	5.7	58	83	175	149	85	7	283	1	14	9	4.04	Louvari 2000
4. Sporades isls																	
650309	5:57	39.30	23.80	7	6.1*	***135***	***85***	***15***	44	75	175	269	7	0	14	14.7	Taymaz *et al.* 1991
920710	16:28	39.19	23.34	11	1.9	200	60	−152	***95***	***66***	***−33***	56	40	149	4		Hatzfeld *et al.* 1999
920710	17:36	39.20	23.32	11	1.4	205	80	−154	110	64	−11	70	26	335	11		Hatzfeld *et al.* 1999
920713	3:44	39.29	23.09	11	1.6	35	60	−160	***295***	***73***	***−31***	252	34	347	8		Hatzfeld *et al.* 1999
920716	2:52	39.11	23.34	12	1.3	60	45	−130	***290***	***57***	***−57***	255	62	357	7		Hatzfeld *et al.* 1999
920722	21:42	39.21	23.47	11	2.0	245	75	161	***340***	***72***	***16***	293	2	202	24		Hatzfeld *et al.* 1999
920722	22:27	39.22	23.49	11	1.7	245	75	161	***340***	***72***	***16***	293	2	202	24		Hatzfeld *et al.* 1999
920723	12:41	39.23	23.54	11	2.3	155	60	−10	***250***	***81***	***−150***	117	28	19	14		Hatzfeld *et al.* 1999
920724	1:06	39.16	23.24	11	2.0	130	50	−36	***245***	***63***	***−134***	104	51	5	8		Hatzfeld *et al.* 1999
920726	1:50	39.24	23.69	10	2.3	60	70	−153	***320***	***65***	***−22***	281	33	189	3		Hatzfeld *et al.* 1999
920727	19:07	39.21	23.21	11	2.4	***70***	***45***	***−166***	330	80	−46	279	38	28	22		Hatzfeld *et al.* 1999

Table 1. (*Continued.*)

Date yr/mo/dd	Origin time h/m/s	Coordinates Lat. N	Long. E	Depth (km)	M	Nodal plane 1 Strike	Dip	Rake	Nodal plane 2 Strike	Dip	Rake	P axis Az	Pl	T axis Az	Pl	Mo *10e17 N m	Ref
920823	2:02	39.30	23.16	8	1.6	140	65	0	**230**	**90**	**−155**	98	17	2	17		Hatzfeld *et al.* 1999
920824	1:22	39.19	23.25	11	1.3	**255**	**30**	**−77**	60	61	−97	312	73	155	16		Hatzfeld *et al.* 1999
920824	11:35	39.22	23.56	11	1.7	275	70	−14	**10**	**77**	**−159**	234	24	142	5		Hatzfeld *et al.* 1999
920824	23:52	39.14	23.30	11	2.2	**340**	**75**	**19**	245	72	164	112	2	203	24		Hatzfeld *et al.* 1999
920825	2:31	39.28	23.13	7	1.6	130	60	−74	**280**	**34**	**−116**	76	70	208	13		Hatzfeld *et al.* 1999
5. Evia Island																	
920709	9:49	38.96	23.13	10	2.5	**250**	**60**	**−144**	140	59	−36	105	46	15	1		Hatzfeld *et al.* 1999
920710	1:30	38.74	23.35	13	2.7	120	60	−49	**240**	**49**	**−139**	83	55	182	6		Hatzfeld *et al.* 1999
920715	8:29	39.01	23.25	10	1.8	275	35	−90	95	55	−90	5	80	185	10		Hatzfeld *et al.* 1999
920716	11:58	38.76	23.34	13	2.2	70	75	161	**165**	**72**	**16**	118	2	27	24		Hatzfeld *et al.* 1999
920718	19:45	38.86	23.35	12	1.6	120	65	−32	225	61	−151	81	40	173	3		Hatzfeld *et al.* 1999
920721	11:08	38.99	23.34	9	1.2	**120**	**60**	**−28**	225	66	−147	84	40	351	4		Hatzfeld *et al.* 1999
920721	15:13	38.70	23.34	13	2.3	120	60	−55	**245**	**45**	**−135**	82	58	186	8		Hatzfeld *et al.* 1999
920722	10:19	38.76	23.36	10	1.7	**55**	**60**	**−152**	310	66	−33	271	40	4	4		Hatzfeld *et al.* 1999
920723	3:35	38.78	23.44	12	1.8	110	80	−26	205	64	−169	65	26	160	11		Hatzfeld *et al.* 1999
920728	10:33	38.87	23.49	14	2.3	230	80	−154	**135**	**64**	**−11**	95	26	0	11		Hatzfeld *et al.* 1999
920729	7:51	38.70	22.90	12	2.3	**240**	**70**	**−153**	140	65	−22	101	33	9	3		Hatzfeld *et al.* 1999
920730	20:05	38.90	22.92	14	1.6	160	70	−14	255	77	−159	119	24	27	5		Hatzfeld *et al.* 1999
920731	16:54	38.79	23.22	11	1.6	120	75	−19	215	72	−164	77	24	168	2		Hatzfeld *et al.* 1999
920806	14:45	38.92	23.43	14	2.3	284	85	22	**192**	**68**	**175**	56	12	150	19		Hatzfeld *et al.* 1999
920807	19:44	38.67	23.37	11	1.7	**120**	**60**	**−20**	220	73	−149	83	34	348	8		Hatzfeld *et al.* 1999
920809	5:09	38.90	23.69	12	2.1	145	50	−23	**250**	**73**	**−138**	116	41	13	14		Hatzfeld *et al.* 1999
920809	14:32	39.01	23.34	7	1.6	**120**	**50**	**−29**	230	68	−136	93	46	351	11		Hatzfeld *et al.* 1999
920818	3:39	38.64	23.53	13	1.8	290	65	22	**190**	**70**	**153**	241	3	149	33		Hatzfeld *et al.* 1999
920820	10:36	38.88	23.39	12	1.8	210	65	−132	95	48	−35	71	51	329	10		Hatzfeld *et al.* 1999
920823	9:36	38.81	23.20	14	2.8	**113**	**60**	**−23**	215	70	−148	77	37	342	6		Hatzfeld *et al.* 1999
920824	1:28	38.58	23.12	15	2.1	130	65	−32	**235**	**61**	**−151**	91	40	183	3		Hatzfeld *et al.* 1999
6. Magnesia basin (Thessaly)																	
800709	2:10	39.23	22.98	1	5.7*	80	43	−78	**244**	**48**	**−101**	89	82	342	3		Papazachos *et al.* 1983
800709	2:11	39.27	23.09	10	6.6*	**58**	**41**	**−128**	283	58	−62	243	65	354	9	86.7	Harvard CMT-solution
800709	2:35	39.16	22.65	18	6.1*	**84**	**40**	**−90**	264	50	−90	174	85	354	5		Papazachos *et al.* 1983
850430	18:14	39.26	22.88	11	5.6*	77	50	−105	280	42	−73	287	78	178	4	3.00	Taymaz *et al.* 1991
920707	8:09	39.25	22.68	13	2.3	90	60	−90	270	30	−90	0	75	180	15		Hatzfeld *et al.* 1999
920709	17:31	39.57	22.74	12	2.7	105	30	−86	280	60	−92	183	75	12	15		Hatzfeld *et al.* 1999
920711	17:49	39.39	22.94	10	2.1	80	45	−97	270	45	−83	265	85	355	0		Hatzfeld *et al.* 1999
920711	21:13	39.38	22.95	10	1.5	90	50	−119	**310**	**48**	**−61**	292	69	200	1		Hatzfeld *et al.* 1999
920711	23:56	39.42	22.81	12	1.7	250	52	−116	**109**	**45**	**−60**	98	69	358	4		Hatzfeld *et al.* 1999
920712	1:46	39.42	22.81	11	1.4	95	40	−88	272	50	−92	167	85	3	5		Hatzfeld *et al.* 1999
920715	0:34	39.26	22.85	9	1.3	95	55	−93	280	35	−86	354	80	187	10		Hatzfeld *et al.* 1999
920717	2:08	39.35	23.02	8	1.2	**300**	**87**	**−59**	35	31	−174	238	40	4	35		Hatzfeld *et al.* 1999
920730	16:46	39.33	22.78	11	2.0	265	60	−103	110	33	−69	143	72	5	14		Hatzfeld *et al.* 1999
920731	20:26	39.24	22.72	10	1.6	80	60	−90	260	30	−90	350	75	170	15		Hatzfeld *et al.* 1999
920731	20:29	39.24	22.72	7	1.5	80	60	−90	260	30	−90	350	75	170	15		Hatzfeld *et al.* 1999
920801	2:32	39.25	22.88	7	1.3	90	50	−114	305	46	−64	293	71	197	2		Hatzfeld *et al.* 1999
920807	6:16	39.40	22.91	9	1.6	**290**	**70**	**−67**	60	30	−136	232	59	3	22		Hatzfeld *et al.* 1999
920809	19:01	39.40	22.81	12	2.1	**233**	**80**	**−127**	130	38	−16	108	43	351	26		Hatzfeld *et al.* 1999
920810	11:58	39.40	22.81	10	2.4	**110**	**50**	**−61**	250	48	−119	88	69	180	1		Hatzfeld *et al.* 1999
920810	14:42	39.37	22.85	11	2.0	280	40	−94	105	50	−87	39	84	193	5		Hatzfeld *et al.* 1999
920814	5:41	39.41	22.80	12	1.6	**295**	**35**	**−78**	100	56	−99	342	77	196	11		Hatzfeld *et al.* 1999
920817	16:54	39.28	22.95	8	1.1	210	25	−158	100	81	−67	35	49	171	32		Hatzfeld *et al.* 1999
920819	20:15	39.34	22.63	12	2.7	85	40	−94	270	50	−87	204	84	358	5		Hatzfeld *et al.* 1999
920819	21:20	39.35	22.62	13	1.8	**70**	**65**	**−139**	320	54	−32	290	46	193	7		Hatzfeld *et al.* 1999
920819	22:11	39.35	22.63	11	2.0	110	25	−62	260	68	−102	149	65	359	22		Hatzfeld *et al.* 1999
920819	23:11	39.36	22.62	12	1.7	100	40	−47	**230**	**62**	**−119**	94	61	341	12		Hatzfeld *et al.* 1999
920821	1:59	39.36	22.62	11	1.8	70	40	−118	285	56	−68	246	70	360	8		Hatzfeld *et al.* 1999
920823	22:06	39.26	22.79	6	1.5	**65**	**70**	**−142**	320	55	−25	288	40	189	9		Hatzfeld *et al.* 1999
7. Lamia (Sperchios basin)																	
830919	1:18	38.74	22.43	8	5.1*	242	52	−100	**78**	**39**	**−77**	109	80	339	7		Burton *et al.* 1995
920714	12:35	38.91	22.49	12	1.9	90	60	−90	270	30	−90	0	75	180	15		Hatzfeld *et al.* 1999
920714	21:08	39.04	22.46	19	1.3	75	40	−98	265	50	−84	215	83	350	5		Hatzfeld *et al.* 1999
920729	11:00	38.98	22.44	14	2.9	90	50	−103	**290**	**42**	**−75**	301	79	189	4		Hatzfeld *et al.* 1999
920804	5:47	38.69	22.68	12	2.1	105	60	−88	280	30	−94	22	75	193	15		Hatzfeld *et al.* 1999

Table 1. (*Continued.*)

Date yr/mo/dd	Origin time h/m/s	Coordinates		Depth (km)	M	Nodal plane 1			Nodal plane 2			P axis		T axis		Mo *10e17 N m	Ref
		Lat. N	Long. E			Strike	Dip	Rake	Strike	Dip	Rake	Az	Pl	Az	Pl		
920807	10:39	38.91	22.50	11	1.9	265	40	−121	123	57	−67	83	68	197	9		Hatzfeld *et al.* 1999
920808	4:00	38.92	22.42	10	2.1	**155**	**−70**	**−64**	280	32	−140	99	57	226	21		Hatzfeld *et al.* 1999
920808	9:30	38.91	22.40	12	1.8	175	70	−38	**280**	**55**	**−155**	132	40	231	9		Hatzfeld *et al.* 1999
920808	22:26	38.98	22.47	15	1.2	95	52	−79	257	39	−104	51	79	177	7		Hatzfeld *et al.* 1999
920813	16:26	38.71	22.67	14	2.2	95	55	−90	275	35	−90	5	80	185	10		Hatzfeld *et al.* 1999
920815	1:47	38.75	22.76	13	2.5	100	35	−86	275	55	−93	174	80	7	10		Hatzfeld *et al.* 1999
920815	3:20	38.74	22.75	13	1.6	**85**	**55**	**−90**	265	35	−90	355	80	175	10		Hatzfeld *et al.* 1999
8. Central Western Anatolia																	
390922	0:36	39.00	27.00	10	6.5	100	51	−70	250	43	−113	71	74	176	4		Ritsema 1974
560220	20:31	39.86	30.49	10	6.5	**141**	**57**	**−50**	264	50	−135	108	57	204	4		McKenzie 1972
680311	18:40	38.81	29.11	23	5.0	46	60	144	156	59	36	101	1	11	46		Zanchi & Angelier 1993
690323	21:08	39.10	28.50	8	6.0	112	34	−90	**292**	**56**	**−90**	202	79	22	11	9.80	Eyidogan & Jackson 1985
690324	1:59	39.11	28.51	30	5.0	**165**	**45**	**−37**	283	65	−129	146	53	40	12		Zanchi & Angelier 1993
690325	13:21	39.20	28.40	8	6.2	90	40	−104	288	51	−79	248	79	10	6	17.00	Eyidogan & Jackson 1985
690328	1:48	38.50	28.50	3	6.6*	**300**	**41**	**−97**	129	49	−84	83	84	215	4	129.00	Braunmiller & Nabelek 1996
690406	3:49	38.50	26.40	16	5.9	116	60	−90	**296**	**30**	**−90**	26	75	206	15		McKenzie 1972
690430	20:20	39.10	28.50	8	5.4	**78**	**39**	**−114**	288	55	−72	247	73	5	8		McKenzie 1972
700328	21:02	39.20	29.50	8	7.1*	**304**	**41**	**−97**	133	49	−84	87	84	219	4	505.00	Braunmiller & Nabelek 1996
700328	23:11	39.12	29.55	33*	5.5	74	32	−110	277	60	−78	216	72	358	14		McKenzie 1978
700329	6:56	39.06	29.74	39	5.1	**40**	**46**	**−135**	275	59	−54	238	59	340	7		Zanchi & Angelier 1993
700330	7:59	39.34	29.26	8	5.0	100	22	−90	280	68	−90	190	67	10	23		Zanchi & Angelier 1993
700416	10:42	38.97	29.92	8	5.6	112	60	−84	280	31	−100	38	74	198	15	2.70	Eyidogan & Jackson 1985
700419	13:29	39.00	29.80	8	6.1	104	34	−90	284	56	−90	194	79	14	11	19.40	Eyidogan & Jackson 1985
700419	13:47	39.03	29.80	19*	5.8	114	24	−90	294	66	−90	204	69	24	21		Zanchi & Angelier 1993
700423	9:01	39.08	28.60	28*	5.6	77	50	−96	**266**	**40**	**−83**	310	83	171	5		McKenzie 1978
710413	12:52	39.03	29.89	13	5.3	120	50	−90	**300**	**40**	**−90**	30	85	210	5		Zanchi & Angelier 1993
710525	5:43	39.07	29.67	6	6.0	96	37	−108	298	55	−77	249	76	19	9	9.50	Eyidogan & Jackson 1985
720314	14:05	39.30	29.46	18	5.6	101	35	−87	277	55	−92	178	80	9	10		McKenzie 1978
790614	11:44	38.80	26.60	8	5.9	105	51	−75	262	41	−108	71	77	184	5	6.70	Taymaz *et al.* 1991
790616	18:42	38.46	26.77	15	5.3	**127**	**45**	**−48**	255	58	−124	112	61	8	7	1.20	Harvard CMT-solution
790718	13:12	39.44	29.19	15	5.3	111	34	−85	285	56	−93	183	79	17	11	1.15	Harvard CMT- solution
940128	15:45	38.67	27.48	14	5.4	114	60	−71	259	35	−120	64	69	190	13	1.14	Louvari 2000
940524	2:05	38.83	26.49	10	5.5	**136**	**49**	**−41**	256	60	−131	113	55	14	6	2.10	Louvari 2000
990725	6:56	38.96	28.19	15	5.2	**151**	**70**	**−25**	250	67	−158	110	31	201	2	0.83	Harvard CMT- solution
9. Southern Western Anatolia																	
550716	7:07	37.66	27.19	6	6.7	55	51	−137	**295**	**58**	**−48**	261	55	356	4		McKenzie 1972
590425	0:26	37.00	28.50	1	6.2	**65**	**76**	**−70**	189	24	−144	359	55	139	28		McKenzie 1972
650613	20:01	37.80	29.30	2	6.0	91	74	−103	**311**	**21**	**−52**	342	59	192	28	8.53	Yilmazturk & Burton 1999
710512	6:25	37.57	29.70	12	5.9	**68**	**56**	**−80**	230	35	−105	10	76	151	11	6.00	Taymaz & Price 1992
710512	10:10	37.60	29.70	5	5.6	**73**	**14**	**−90**	253	76	−90	163	59	343	31		Papazachos *et al.* 1991
710512	12:57	37.60	29.60	12	5.7	53	25	−92	235	65	−89	147	70	324	20	2.50	Taymaz & Price 1992
710909	15:10	37.30	30.24	34	5.6	**160**	**90**	**173**	250	83	0	205	5	115	5	2.21	Yilmazturk & Burton 1999
760819	1:12	37.70	28.89	4	6.1	164	45	−30	276	69	−131	142	49	35	14	14.80	Yilmazturk & Burton 1999
861011	9:00	37.91	28.53	8	5.7	80	67	−128	**323**	**44**	**−35**	304	52	197	13	4.35	Louvari 2000
890224	0:40	37.76	29.44	15	5.3	**113**	**39**	**−77**	276	52	−101	141	79	14	7	1.11	Harvard CMT- solution
890427	23:06	37.10	28.20	7	5.4	**114**	**35**	**−71**	271	57	−103	145	74	10	11	1.12	Louvari 2000
890428	13:30	37.06	28.01	12	5.5	**107**	**44**	**−57**	245	54	−118	97	67	354	5	1.55	Louvari 2000
900718	11:29	37.04	29.51	14	5.4	53	55	−113	**270**	**41**	**−60**	270	70	159	7	1.40	Louvari 2000
921106	20:06	38.02	26.97	6	6.0	146	76	13	53	77	166	100	1	9	19	10.87	Louvari 2000
941113	6:56	37.12	28.02	15	5.4	139	36	−83	310	54	−95	198	80	44	9	1.33	Harvard CMT- solution
951001	15:57	38.06	30.13	4	6.3*	**136**	**43**	**−87**	312	47	−93	179	87	44	2	31.00	Wright *et al.* 1999

Table 1. (*Continued.*)

Date yr/mo/dd	Origin time h/m/s	Coordinates		Depth (km)	M	Nodal plane 1			Nodal plane 2			P axis		T axis		Mo ∗10e17 N m	Ref
		Lat. N	Long. E			Strike	Dip	Rake	Strike	Dip	Rake	Az	Pl	Az	Pl		
960402	7:59	37.84	26.87	9	5.4	**124**	**46**	**−57**	261	53	−119	110	67	11	4	1.14	Louvari 2000
970121	20:47	37.98	28.33	18	5.2	85	28	−138	**317**	**72**	**−68**	256	58	30	24	0.78	Harvard CMT- solution
980404	16:16	38.10	30.16	15	5.2	154	46	−75	313	46	−105	144	79	234	0	0.86	Harvard CMT- solution

of the NAF into the Marmara Sea is still on-going (see LePichon *et al.* 2001); several scientists favour a segmented pull-apart fault geometry, indicating a transtensional tectonic regime, over a strike-slip regime.

No fault plane was assumed known and the results of the inversion are summarised in Fig. 3(b). The geometry of the stress tensor indicates oblique motion-normal faulting with a considerable strike-slip component. σ_{Hmax} trends WNW–ESE (N145°E) as in the NAF. The distribution of R-values shown in the right of Fig. 3(b), which have a tendency towards values larger than 0.5, and the R-value for the best fitting model (0.7) is the signature of some reverse faulting observed in the area (i.e. events of March 3, 1969; July 5, 1983 among others). This reverse faulting is probably accommodating a small shortening component on mainly NE–SW trending faults whose main motion is strike-slip and this is reflected in the stress tensor, as well.

3.3 North Aegean Sea

As the NAF enters into the Aegean Sea, it branches into two main segments. The northern branch passes between the islands of Samothraki and Imvros, north of Lemnos and ends up at the Sporades basin. The southern branch, bathymetrically less pronounced and less active, passes north of Lesbos and ends near the eastern coast of Evia Island. From the 18 focal mechanisms, for four the fault plane was known. For the 1968 February 19, Agios Efstratios event, the rupture plane was identfied by Pavlides & Tranos (1991), for the 1981 December 19, the 1982 January 18, and 1983 August 6, events, the aftershock sequences, studied by Roccæt *al.* (1985) and Kiratzi *et al.* (1991), define the fault planes. For all four events the NNE–SSW trending plane with a dextral strike-slip component was the fault plane. The inversion resulted in a pure strike-slip stress tensor (Fig. 3c), with σ_{Hmax} trending E–W, σ_3 trending N–S and an R-value equal to 0.5.

There is no strong normal component in the resolved stress tensor as I would expect, which indicates that the strike-slip motion transferred from the NAF prevails and controls the stress regime in the Northern Aegean area. Actually, except from the 1967 March 4, event (Fig. 2a) that shows normal faulting, all other focal mechanisms show strike-slip motions. The recent earthquake that occurred on 2001 July 26 near Skyros Island (39.1°N, 24.3°E; **M** 6.4) has also strike-slip mechanism (NP1: Strike 145, dip 80°, rake 8°; NP2: strike 54°, dip 82°, rake 170°, Benetatos *et al.* 2002). Thus, the evidence so far indicates that the deformation in the Northern Aegean Sea, south of the three-leg Chalkidiki peninsula up to the northern boundary of the Cyclades Islands, is mainly taken-up by strike-slip faulting.

3.4 Sporades Islands

The Sporades basin marks the westernmost part of the North Aegean Trough, where the Sporades Islands are situated. The bathymetry of the basin is dominated by faults trending NW-SE and NE–SW. The largest instrumentally recorded event is the 1965 March 9 event (**M** 6.1). No fault plane was known *a priori*. The inversion of 16 focal mechanisms resulted in a steeply dipping σ_2 (65°) and shallow dipping σ_1 and σ_3 axes (Fig. 3d), a characteristic strike-slip regime. σ_{Hmax} keeps the same E–W orientation as in the Northern Aegean Sea.

3.5 Evia Island

The study area covers the northern part of Evia Island as well as the Northern Evoikos Gulf (Fig. 2b), a gulf similar in size with the Gulf of Corinth. The Northern Evoikos Gulf is an asymmetric half-graben. In this region no large events occurred during instrumental time, so only microearthquake data could be used for the inversion.

The focal mechanisms clearly indicate strike-slip motions, combined with normal components. The strike-slip faulting is also crossing the North Evoikos Gulf and reaches the coasts of Greece. Fig. 2 shows that the shear motion is penetrating up to the 22.9E meridian. West of that meridian the normal faulting system is prevailing. For Evia Island one question that arises is whether the focal mechanisms, from small magnitude events, reflect the regional stressfield. Previous work has shown that, in general, the mean focal mechanism obtained from microearthquakes does reflect the regional stressfield (Louvari 2000). In addition, recently determined fault-plane solutions for earthquakes in the southern part of Evia Island indicate strike-slip faulting, as well (Panagiotou 2001). Until we have data from large events, the evidence we have from small magnitudes events indicate that the deformation at the island of Evia is taken up by strike-slip faulting combined with normal components of motion.

This transtensional character is also evident from the directions of the principal stress axes, the steeply dipping (75) σ_2 axis (Fig. 3e) and the stress ratio (R = 0.3), listed in Table 2. Once again, σ_{Hmax} trends ~E–W, the same trend as in Sporades Islands and North Aegean Sea.

3.6 Magnesia basin (Thessaly)

From a morphotectonic point of view, Thessaly represents an alternation of NW trending structural lows and highs dissected by NNW and ENE trending faults (Drakos *et al.* 2001). This region has been the site of many large earthquakes in the past. The Volos 1980 July 9 (**M** 6.6) seismic sequence, which occurred in the Almyros plain (Fig. 2b) is the most recent event. For two earthquakes out of 28 used in the inversion, the fault plane was known *a priori*. Based on the surface expression of the fault, the spatial distribution of the aftershocks and the inversion of levelling data, the south dipping planes were assumed fault planes for the 1980 mainshock and its largest aftershock (Papazachos *et al.* 1983; Drakos *et al.* 2001). The principal stress axes (Fig. 3f) indicate normal faulting (σ_1 steeply dipping) with axis σ_3 keeping the regional N–S trend and σ_{Hmax} trending ~E–W. However, across the path from the Sporades Islands to Magnesia, axes σ_1 and σ_2 have 'flipped' (Figs 3d and f) even though they retain

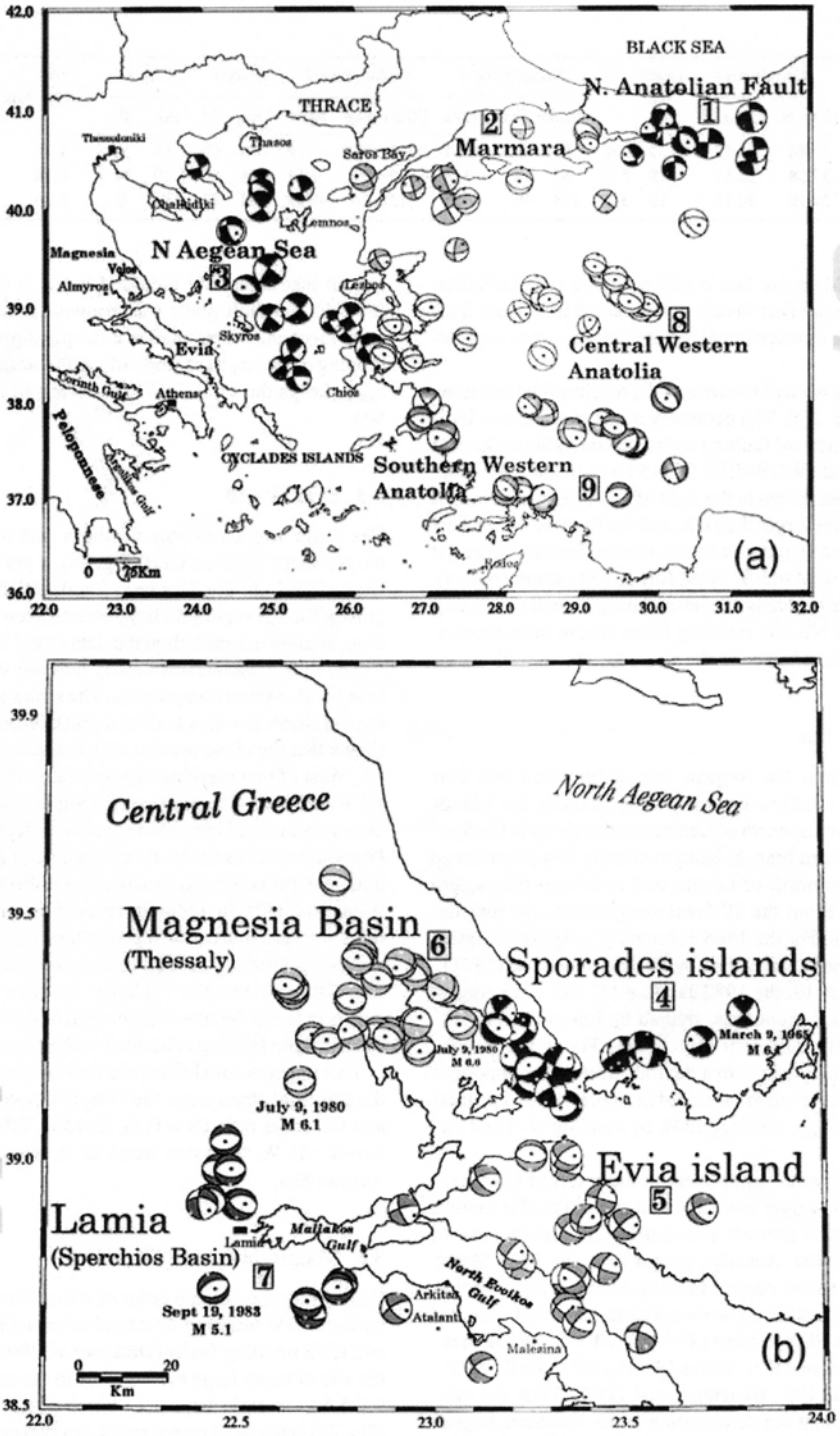

Figure 2. (a) Distribution of fault-plane solutions for earthquakes with epicentres along the North Anatolian Fault, its Aegean Sea strands as well as Western Anatolia (regions 1, 2, 3 and 8, 9 in Tables 1 and 2). (b) Distribution of fault-plane solutions for earthquakes with epicentres in central Greece along the end point of the NAFZ in the Aegean Sea. Different beach-ball shading is used to denote the different regions, which are numbered as in Table 1. (In Fig. 2a beach-balls are scaled relative to earthquake magnitude. In Fig. 2b all have the same size but strong earthquakes are identified by date.)

Table 2. Regional stress tensor inversion results for the subregions studied.

Region	Average misfit, F(°)	σ_1		σ_2		σ_3		R	N	σ_{Hmax}
		Az°	Plunge°	Az°	Plunge°	Az°	Plunge°			
N. Anatolian F.	3.3	126	3	269	86	35	3	0.5	11	126
Marmara	5.2	321	46	149	44	55	4	0.7	12	145
N Aegean Sea	5.2	274	4	147	83	4	5	0.5	18	274
Sporades Islands	4.3	95	6	199	65	2	24	0.4	16	95
Evia Island	4.1	87	14	267	75	357	0	0.3	21	87
Magnesia basin (Thessaly)	3.7	178	75	269	0	359	15	0.3	28	269
Lamia (Sperchios basin)	2.8	33	58	283	12	186	29	0.2	12	283
Central Western Anatolia	3.5	189	67	280	0	10	23	0.5	26	280
Southern Western Anatolia	4.8	227	77	57	13	327	2	0.4	19	57

Region—as defined in Fig. 2(A), B; F—average mis fit angle; σ_1—maximum compressive stress; σ_2—intermediate principal stress; σ_3—minimum compressive stress; R—measure of relative stress magnitudes $\{R = (\sigma_2 - \sigma_1)/(\sigma_3 - \sigma_1), (0 < R < 1)\}$; N—number of focal mechanisms used in the inversion; σ_{Hmax}—orientation of the axis of maximum horizontal compression (following Zoback 1992).

the same orientations. Thus, Magnesia forms an area of progressive transition from strike-slip faulting to normal faulting and the style of deformation is transtensional.

3.7 Lamia (Sperchios basin)

The Sperchios basin is bounded by a major fault system that borders also the south coasts of the North Evoikos Gulf and continues to Arkitsa (Figs 2b and 5c). No large instrumentally recorded events occurred in this area. However, the town of Lamia (known as Zitouni at that time) and nearby villages were severely affected by a strong earthquake (**M** 6.6), which occurred during the night of October 4, 1740 (Papazachos & Papazachou 1997).

No fault planes were assumed known *a priori*, and the largest event used is the September 19, 1983 with **M** 5.1 (Burton *et al.* 1995). The best fitting model (Fig. 3g) corresponds to a normal faulting stress tensor. The σ_3 axis trends ~N–S, and the direction of σ_{Hmax} is E–W, as for the Magnesia basin.

3.8 Central Western Anatolia

Central and Southern Western Anatolia are dominated by a number of grabens with variable orientations (E–W or NE–SW or NW–SE). Normal faults bound the northern and southern sides of these grabens. The most pronounced structures are the Simav Graben and the Gediz Graben corresponding to the extended graben system north of the Menderes Massif between Manisa and Alaşehir (see Fig. 4).

26 fault-plane solutions were available and for two of those the fault plane was assumed known *a priori*. For the March 28, 1969 Alaşehir **M** 6.6 event and for the March 28, 1970 Gediz **M** 7.1 event. Both events produced extended surface ruptures along NW SE trending and toward NE dipping faults (Ambraseys & Tchalenko 1970; Eyidoğan & Jackson 1985; Braunmiller & Nábělek 1996). The resulting stress tensor (Fig. 3h and Table 2) corresponds to a transtensional regime, with σ_3 striking ~N–S (N10°E). The 90 per cent confidence regions are well separated and narrow. The direction of σ_{Hmax} is ~E–W.

3.9 Southern Western Anatolia

Southern Western Anatolia is structurally dominated by predominantly NE–SW striking faults; a second NW-SE striking fault system is also present. A large number of significant earthquakes during the last century occurred along the NE-SW trending Fethiye–Burdur fault zone. The fault zone is characterized by normal faulting combined with left lateral strike-slip motion (Taymaz & Price 1992).

Nineteen fault-plane solutions were used in the inversion. Only the fault plane of the 1995 October 1 Dinar event was assumed known *a priori*, striking NW–SE and dipping to the SW (Pinar 1998; Wright *et al.* 1999; Koral 2000). The Dinar event occurred at the NW–SE striking Dinar-Çivril fault located at the northeastern end of the Fethiye-Burdur fault zone (see Fig. 4 for locations). The 1971 May 12 Burdur event had no clear surface breaks, only cracks have been reported; it is not clear whether the SE (McKenzie 1978) or the NW (Taymaz & Price 1992) dipping plane is the fault plane. I did not assume the fault plane known for this event. However the SE dipping plane is in better agreement with the resolved stress tensor than the NW dipping plane.

The inversion results (Fig. 3i and Table 2) confirm the tensional character of faulting in Southern Western Anatolia. The stress tensor is well resolved as the areas defined by the limits of the orientations of σ_1 and σ_3 do not overlap. The direction of σ_3 is NW–SE and of σ_{Hmax} is N57°E.

4 ORIENTATION OF THE NODAL PLANES WITH THE SMALLER ANGULAR ROTATION

As I have previously mentioned, choosing the correct fault plane from the two nodal planes is a major problem encountered in the stress tensor inversion schemes of earthquake focal mechanisms. The selection criteria are important because the resulting stress tensor depends on the chosen fault planes. In the lack of other criteria (geological, aftershocks etc) a common approach to solve this problem is to let the inversion algorithm choose the fault planes. This is also followed in the method of Gephart & Forsyth (1984). The idea is that the fault plane is the nodal plane with the smaller misfit (angular rotation) in the tested stressfield. The reader should refer to the work of Michael (1987) and of Lund & Slunga (1999) for a discussion on the reliability of this fault picking technique. Lund & Slunga (1999) tested the advantages and disadvantages of the method thoroughly. They concluded that the algorithm of Gephart & Forsyth (1984) does not always pick the correct nodal plane as fault plane; in some cases the auxiliary plane is picked as fault plane.

In an attempt to see whether the nodal planes, which the inversion algorithm inferred as fault planes, are in general agreement with previous knowledge of the seismotectonic regime, I have done some

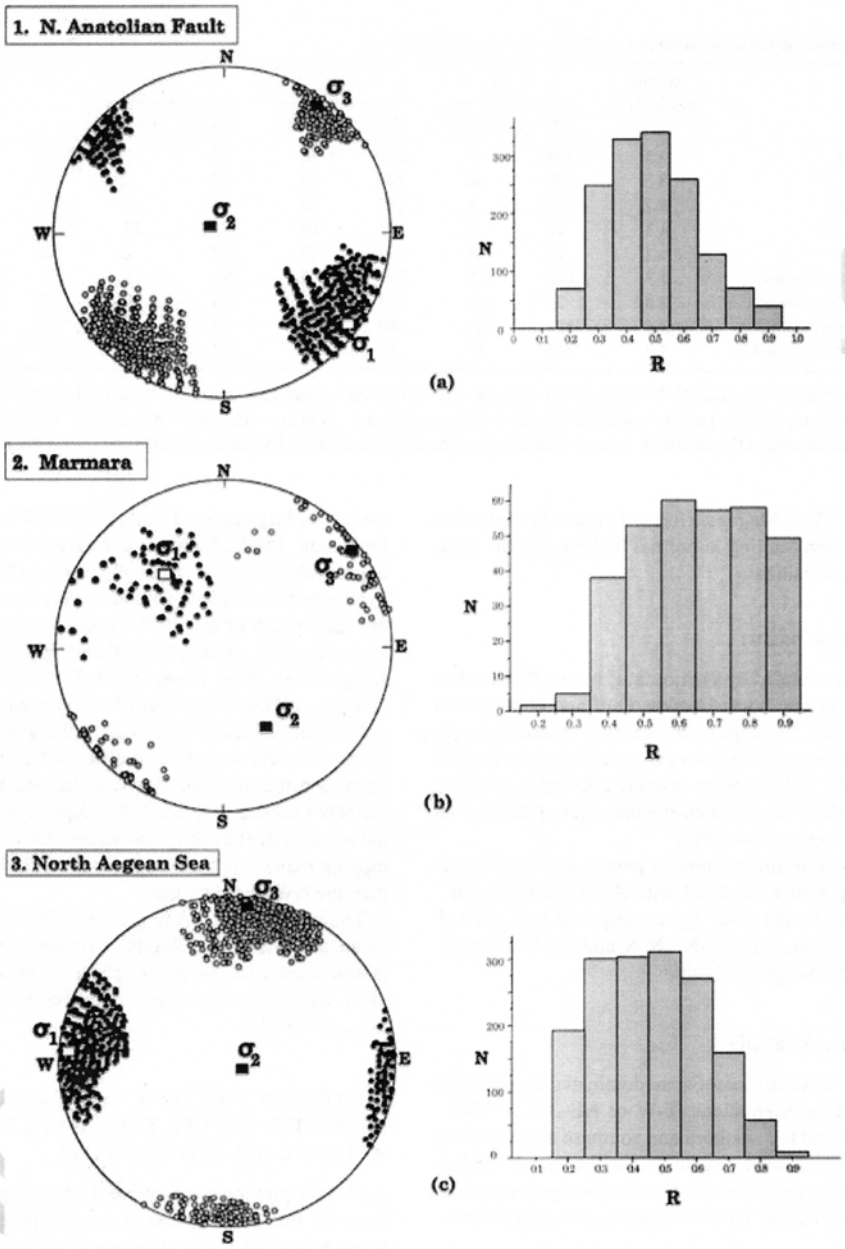

Figure 3. (a)–(i) Orientation of principal stresses, for regions 1– 9 (Fig. 2) together with the 90 per cent con fidence limits for σ_1 and σ_3. The insets show the distribution of R-values for models within the 90 per cent confidence limits.

further investigations. First of all, for the 12 events with known fault plane the algorithm succeeded to pick the correct plane in 9 cases (75 per cent). From the 163 focal mechanisms used in this study the previously mentioned conditions for an optimum choice of the fault plane were fulfilled in 104 cases (64 per cent). In the following I will call these algorithm-selected fault planes as 'inferred fault planes' and further examine their orientation and spatial distribution.

Fig. 4 shows the 'inferred fault planes' for the North Anatolian fault zone and its continuation in the Northern Aegean Sea and for western Anatolia (as in Fig. 2a). The focal mechanisms for some of these events are plotted for comparison. The 'inferred fault planes' follow the general trend of the North Anatolian Fault zone and its continuation in Northern Aegean Sea. The algorithm successfully predicted the N dipping plane for the October 6, 1964 Manyas event (located between the two lakes in the southern coast of the Marmara Sea). This event is known to have produced~40 Km of surface breaks along a north dipping normal fault (Taymaz *et al.* 1991). The NE dipping fault plane for the 1963 September 18 Çınarcık event (Nalbant *et al.* 1998) was also successfully predicted. However, the algorithm failed to choose the fault plane for the 1953 March 18 Yenice-Gönen event and the 1967 May 26 Abant event, both of which are known to have produced NE-SW trending surface ruptures.

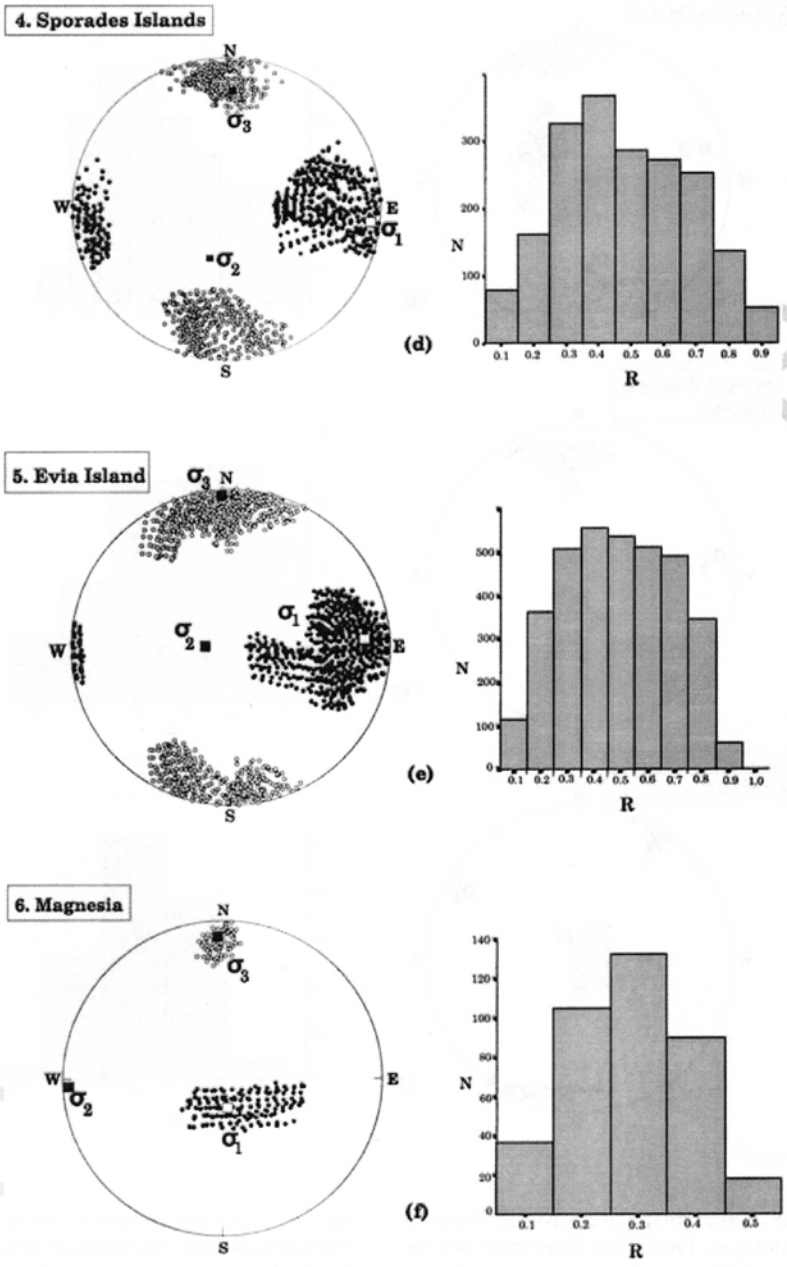

Figure 3. (*Continued.*)

In Central Western Anatolia the general trend of the 'inferred fault planes' is WNW–ESE. This trend changes in southernmost western Anatolia, at the site of Kerme graben, to become ENE-WSW as indicated by the inferred fault planes for the 1959 April 25 (Kerme graben) and 1971 May 12 (Fethiye-Burdur) events. In this southernmost part of Anatolia the T-axes mainly have a NW-SE or NNW–SSE direction. The same direction is widely observed in the inner eastern part of the Hellenic arc, near the island of Rodos (Papazachos *et al.* 1986; Papazachos *et al.* 1998; Louvari 2000).

Fig. 5 shows the 'inferred fault planes' at the western termination of the NAF zone. These fault planes were separated into two categories according to their sense of strike-slip motion; those with a dextral strike-slip component plotted in Fig. 5(a) and those with a left lateral strike-slip component plotted in Fig. 5(b). The general observation that the strike-slip motion terminates gradually as it enters the basins of Greece, where E-W normal faulting is observed, has already been made Hatzfeld *et al.* (1999). This is also shown in Fig. 5(a) and (b). The insets show the horizontal projection of the fault plane and of the slip vectors, which have NE-SW (~N40°) orientation when associated with dextral strike-slip motions and NW–SE (~N320°) orientation when associated with sinistral strike-slip motions. Fig. 5(b) infers that the sinistral strike-slip motion is connected with NW-SE trending structures inherited from past alpine deformations. These structures can be reactivated as dip-slip

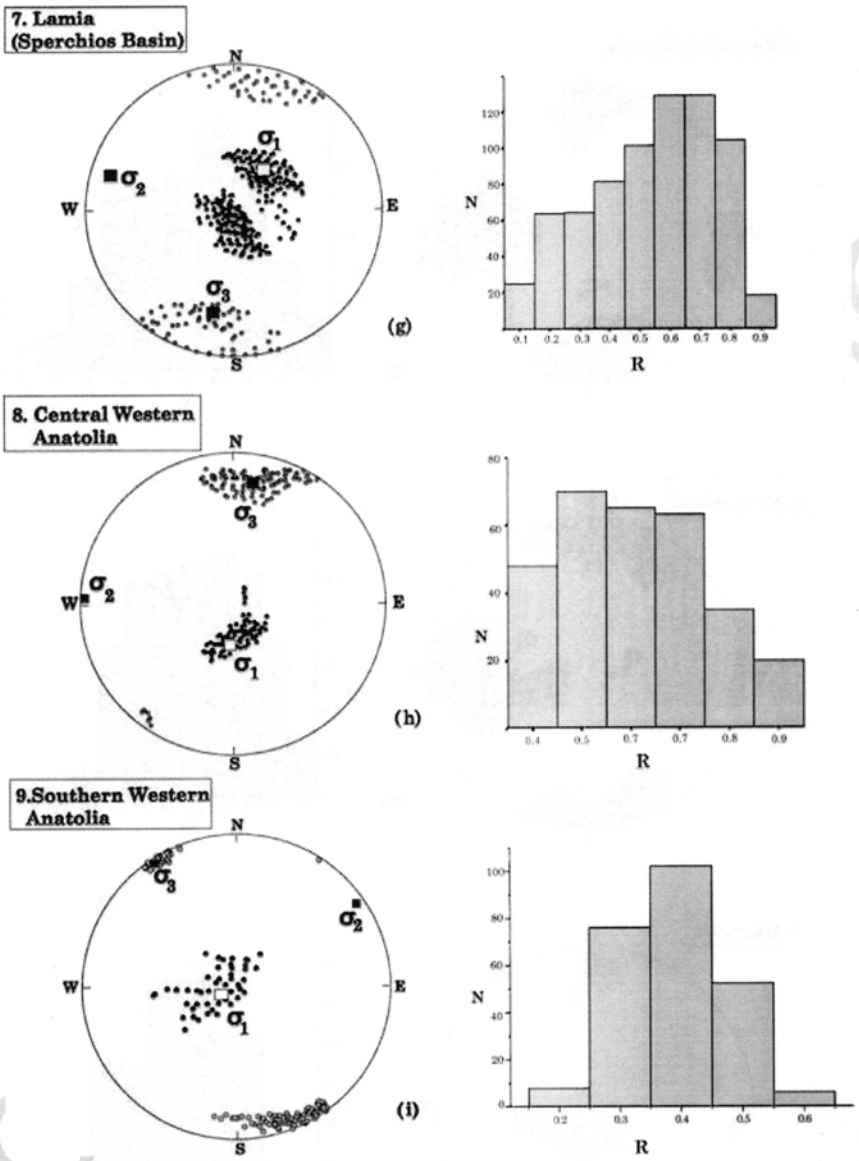

Figure 3. (*Continued.*)

faults with a considerable sinistral strike-slip component (Tranos & Mountrakis 1998; Pavlides *et al.* 1990). This observation will be further investigated using additional evidence.

5 EVIDENCE FOR REACTIVATION OF THE OLD NW–SE TRENDING STRUCTURES

While this paper was in review process, a strong earthquake occurred south of the Sporades Islands whose mechanism and aftershock distribution is shown at the inset of Fig. 4. This event occurred on 2001 July 26, had magnitude**M** 6.4 and epicentral coordinates 39°N–24°E (at the edge of Fig. 5). This event was well recorded by the Greek networks. The distribution of the aftershocks within a few hours after the mainshock (National Observatory of Athens http://www.gein.noa.gr/index-en.html), the waveform and slip distribution modelling (Benetatos *et al.* 2002; Roumeliotie *et al.* in prep.) clearly show that this event was the result of the activation of a NNW–SSE striking fault with a sinistral strike-slip component. The occurrence of this event provided, for the first time, strong seismological evidence for sinistral strike-slip faulting at the termination of the NAF.

Fig. 5(c) shows the major Quaternary and Pliocene faults of central Greece where the E–W normal faults and the NW-SE trending structures bounding the Pilion peninsula, the eastern coast of Evia Island and the North Evoikos Gulf are evident. Indirect evidence for reactivation of the NW-SE structures comes also from macroseismic data. Fig. 5(d) shows the orientation of the major axis of synthetic isoseismals (Papazachos *et al.* 1997) for some past large events. At the area of Pilion peninsula, where the inferred fault planes with

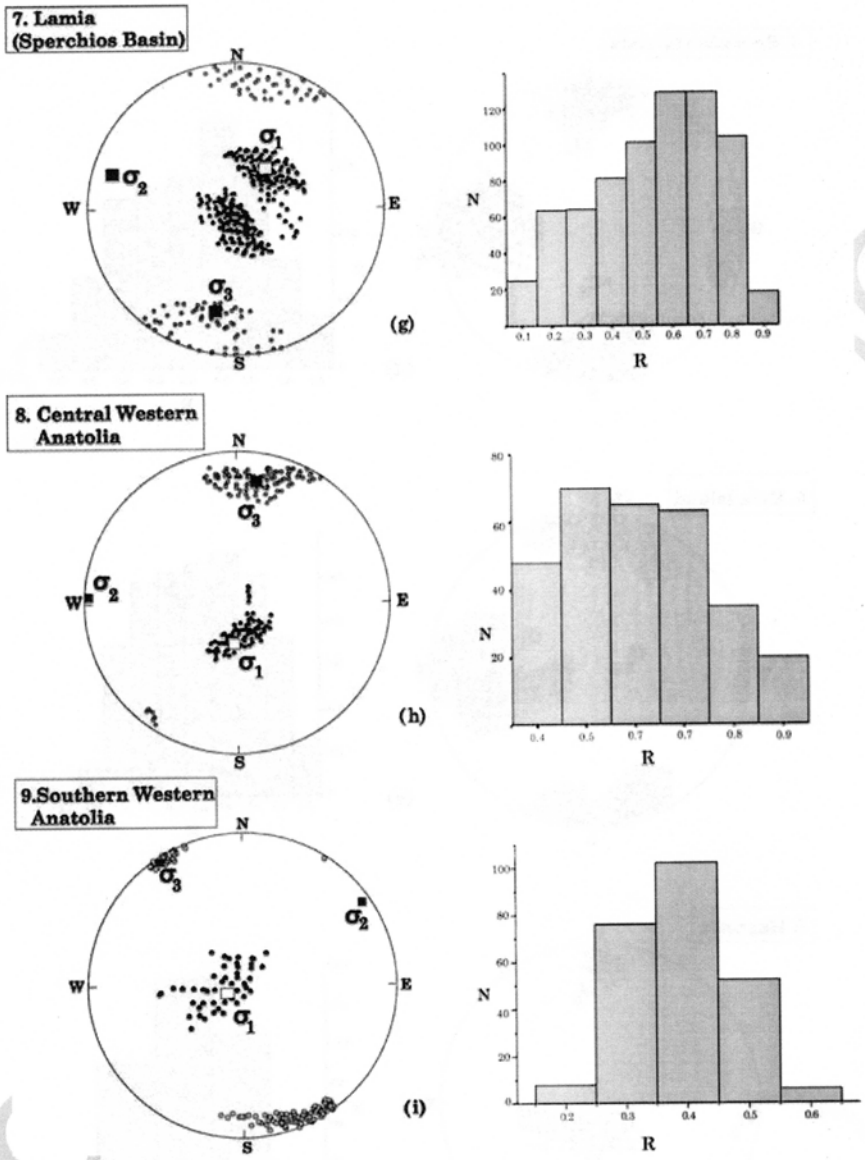

Figure 3. (*Continued.*)

faults with a considerable sinistral strike-slip component (Tranos & Mountrakis 1998; Pavlides *et al.* 1990). This observation will be further investigated using additional evidence.

5 EVIDENCE FOR REACTIVATION OF THE OLD NW–SE TRENDING STRUCTURES

While this paper was in review process, a strong earthquake occurred south of the Sporades Islands whose mechanism and aftershock distribution is shown at the inset of Fig. 4. This event occurred on 2001 July 26, had magnitude**M** 6.4 and epicentral coordinates 39°N–24°E (at the edge of Fig. 5). This event was well recorded by the Greek networks. The distribution of the aftershocks within a few hours after the mainshock (National Observatory of Athens http://www.gein.noa.gr/index-en.html), the waveform and slip distribution modelling (Benetatos *et al.* 2002; Roumeliotie *et al.* in prep.) clearly show that this event was the result of the activation of a NNW–SSE striking fault with a sinistral strike-slip component. The occurrence of this event provided, for the first time, strong seismological evidence for sinistral strike-slip faulting at the termination of the NAF.

Fig. 5(c) shows the major Quaternary and Pliocene faults of central Greece where the E–W normal faults and the NW-SE trending structures bounding the Pilion peninsula, the eastern coast of Evia Island and the North Evoikos Gulf are evident. Indirect evidence for reactivation of the NW-SE structures comes also from macroseismic data. Fig. 5(d) shows the orientation of the major axis of synthetic isoseismals (Papazachos *et al.* 1997) for some past large events. At the area of Pilion peninsula, where the inferred fault planes with

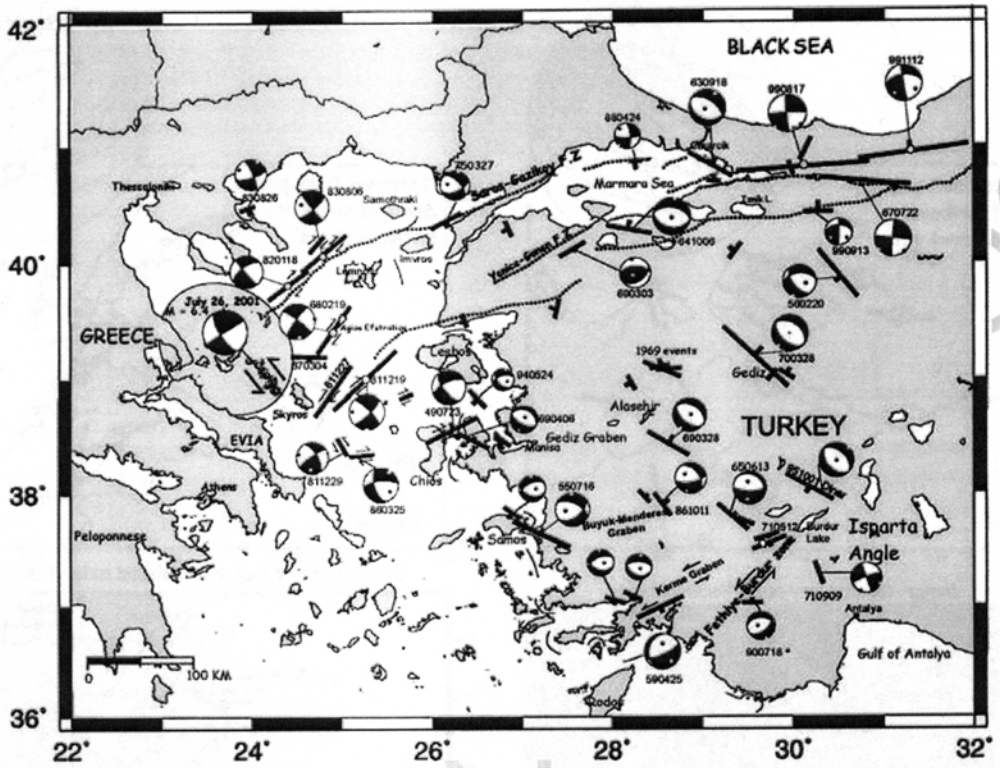

Figure 4. Orientation of fault planes (black thick lines) and sense of dip (small black line) as resolved from the stress tensor analysis ('inferred fault planes' as mentioned in the text) for the regions of western Anatolia, the NAF and its continuation into the Aegean Sea (as shown in Fig. 2a). For graphical present ation only, the length of the line is scaled according to the magnitude of the events. The focal mechanisms of some large events are plotted for comparison (scaled according to magnitude as well). Dotted lines mark the main segments of the NAF zone. The general trend of the NAFZ is well depicted. In western Anatolia the fault planes tend to align in a WNW–ESE direction in the central part and in an ENE– WSW direction in the southernmost part. The inset shows the focal mechanism of the Skyros 2001 July 26 (**M** 6.4) event and its aftershock distribution, indicating the activation of a NW –SE striking plane with sinistral strike-slip component, which was not included in the analysis but is discussed in the text.

sinistral strike-slip motion are aligned (Fig. 5b), the azimuth of the major isoseismal axis for the strong events of March 31, 1930; April 19 and 20, 1955 has a NW-SE trend, which implies motion along this line. The angular difference between the isoseimal axes with a NE–SW orientation and of those having a NW-SE orientation is approximately 90° as in the case of the slip vector orientations (insets of Figs 5a and b).

6 CONCLUSIONS AND DISCUSSION

The method of Gephart & Forsyth (1984) was used to determine regional stresses along the NAF zone and its westward continuation in the Northern Aegean Sea, as well as in central and Southern Western Anatolia. The region was separated into 9 subareas and 163 fault-plane solutions were used in total. In all cases the stress is homogeneously distributed, as the values of average misfit range from 3° to 5°. R-values are in the range of 0.2 to 0.7, and in all cases the 90 per cent confidence limits for σ_1 and σ_3 are separated and the stress tensor is well resolved.

Fig. 6(a) compares the mean focal mechanisms, normalized average of the fault-plane solutions, and the focal mechanism corresponding to the stress tensor, for each subregion studied. The agreement is satisfactory in most of the cases. There is a mismatch in the Marmara area where the normalised average of the focal mechanisms indicates strike-slip motion and the resolved stress tensor corresponds to a focal mechanism indicating oblique strike-slip motion with a strong normal component. The R-value for Marmara area (0.7) has the signature of a transpressional regime and indeed this area is accommodating a component of shortening which is reflected in the focal mechanisms as well. The black arrows in Fig. 6(a) are the horizontal projections of the slip vectors obtained from 'double couple' mechanisms corresponding to the stress tensor. Only the slip vectors from strike-slip faults are plotted. The slip vectors show the extrusion of Anatolia towards the Aegean; their directions are in very good agreement with the GPS velocity vector directions (McCluskyet *al.* 2000) shown in the inset of Fig. 6(a).

Strike-slip motions characterise the stress regimes for the westernmost part of the NAF zone, the Sea of Marmara, the Northern Aegean Sea, the Sporades basin and northern Evia Island. Especially for the island of Evia the resolved stress tensor and recent work (Panagiotou 2001) has shown extensive strike-slip faulting, whereas the dominant structures bounding the island are normal faults. No information is available from the focal mechanism of a large earthquake and I guess unless we have data available from strong events any conclusions concerning the present style of deformation of Evia would be premature.

The stress regimes in the basins of Magnesia and Lamia are characterized by transtension with σ_3 trending ~N–S. Transtension is also characterising Central and Southern Western Anatolia; the σ_3

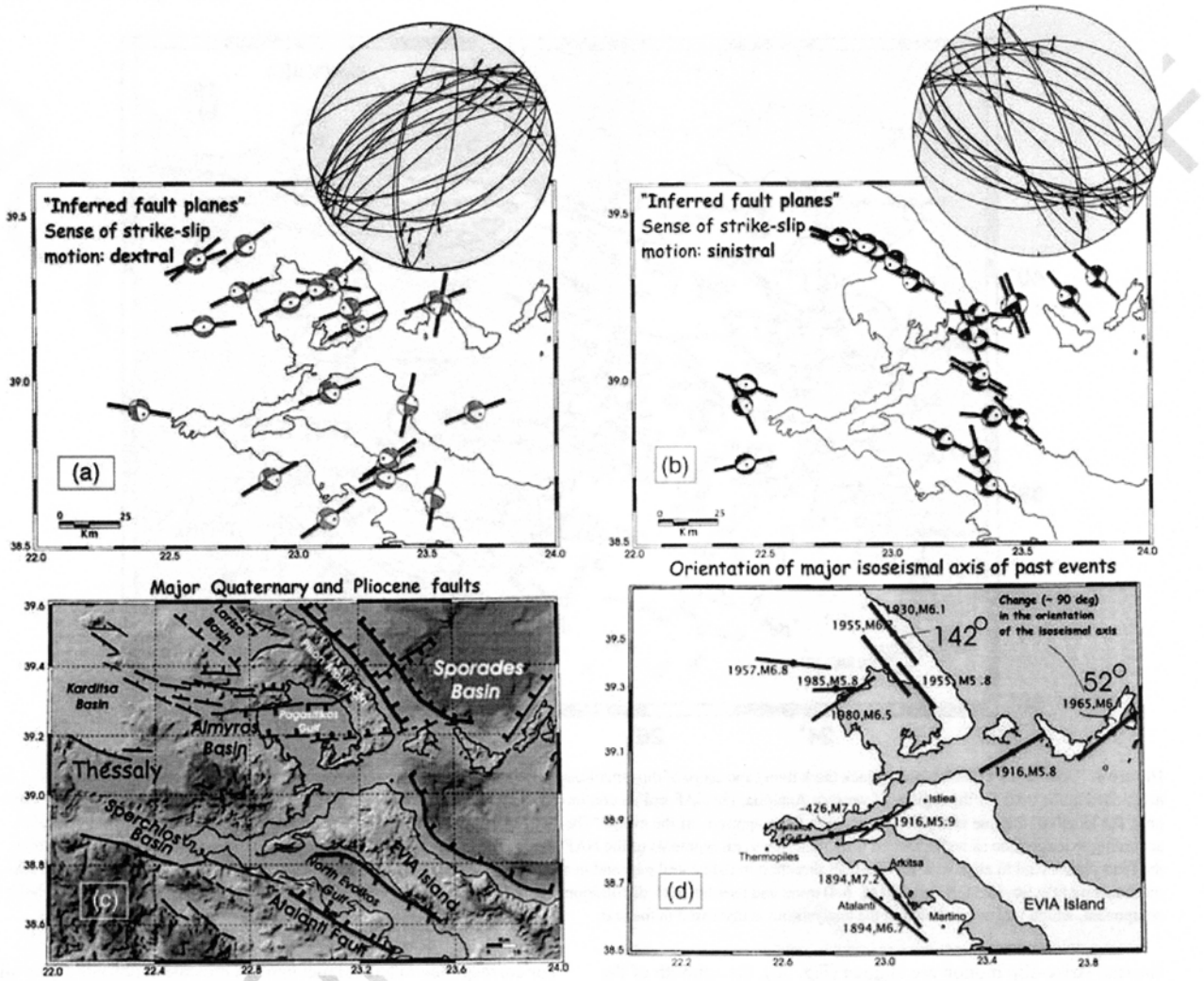

Figure 5. Distribution of 'inferred fault planes' for the area marking the termination of the NAFZ in central Greece (as shown in Fig. 2B). (a) Fault planes with a dextral strike-slip component (b) Fault planes with a left lateral strike-slip component (c) major Quaternary and Pliocene faults (modified from Louvari 2000) and (d) orientation of the major axis of synthetic isoseismals (Papazachos *et al.* 1997) for past events (from Louvari 2000). Note the ~90° change in the orientation of the isoseismals at the area of the Sporades basin (see text for more details). The insets in Figs 5(a) and (b) represent lower hemisphere horizontal projections of the 'inferred fault planes' and the associated slip vectors.

axis trends N10°E in Central Western Anatolia while in Southern Western Anatolia σ_3 is rotated clockwise to N35°W.

At the termination of the NAF against central Greece the NE-SW shear reaches up to the Pilion peninsula, crosses the northern part of the Evia Island, up to 22.9°E meridian (see Fig. 6b). This is expressed from the extended right lateral strike-slip faulting combined with normal components of motion as we approaching central Greece. There are converging indications that the old NW-SE trending structures bounding the Pilion Mountain and Northern Evia are involved in the deformation process and could be activated, under the present-day stressfield, as left lateral strike-slip faults or as normal faults with a left lateral strike-slip component. The shear motion is partitioned along these faults with components parallel and normal to the faults depending on their orientation in respect to the resolved σ_3 axis. In the cases of faults with small angle in respect to σ_3 the shear component is considerable. In the cases of faults with large angles in respect to the resolved σ_3 gravity is more important and the normal component is strong. The occurrence of the recent 2001 July 26 Skyros earthquake (M6.4), with an epicentre south of the Sporades basin, and its clear connection to a NW-SE striking fault with left-lateral strike-slip component supports the existence of left-lateral strike-slip motion as one approaches Greece from the East.

Left lateral strike-slip motion along NW-SE trending structures is in agreement with the broken-slats model of Taymaz *et al.* (1991), the ideas of McKenzie & Jackson (1986) that involve rotations about vertical horizontal axes in central Greece, physical experimental simulations (Gautier *et al.* 1999), and geodetic modelling of strain rate partitioning along major structures (Kahle *et al.* 2000). The complexity of fault geometries observed at the termination of the NAF zone at the Sporades trough is obviously the result of the superimposition of the central Greece extensional tectonics with the

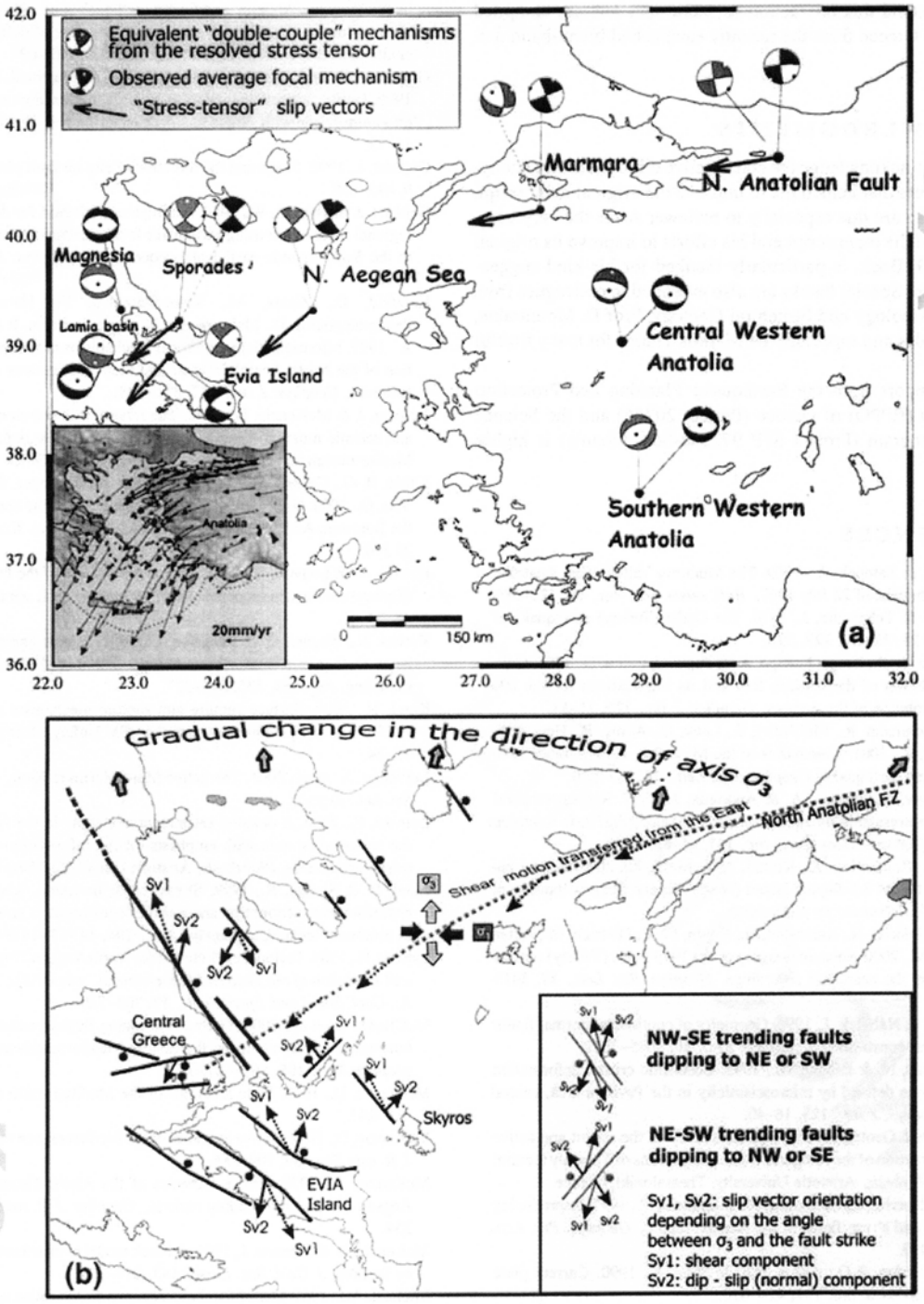

Figure 6. (a) Comparison of the double-couple mechanism corresponding to the regional stress tensor and of the average focal mechanism for each area. In most cases the agreement is very good indicating that the resolved stress tensors, obtained from the inversion of earthquake data at various scales, r eflect regional tectonics. Black arrows are slip vectors, corresponding to the 'stress tensor' mechanisms. The NE–SW trending planes connected with dextral strike-slip motion were taken as the fault planes along the NAF and its continuation in the N. Aegean Sea. The extrusion of the Anatolian plate towards the Aegean is clearly shown by the direction of these slip vectors which are in agreement with the GPS velocity vectors in a Eurasia fixed reference frame shown for comparison in the inset (data from McClusky *et al.* 2000). (b) A representation of the partition of shear motion in the NAF –central Greece interaction zone, showing the geometry of faults and the orientation of slip vectors (arrows). Depending on the fault strike in respect to the resolved σ_3 axis the normal or strike-slip component of motion is defined. Slip vectors associated with predominant normal components of motion are shown with straight lines whereas slip vectors associated with predominant strike-slip components of motion are shown with dashed lines.

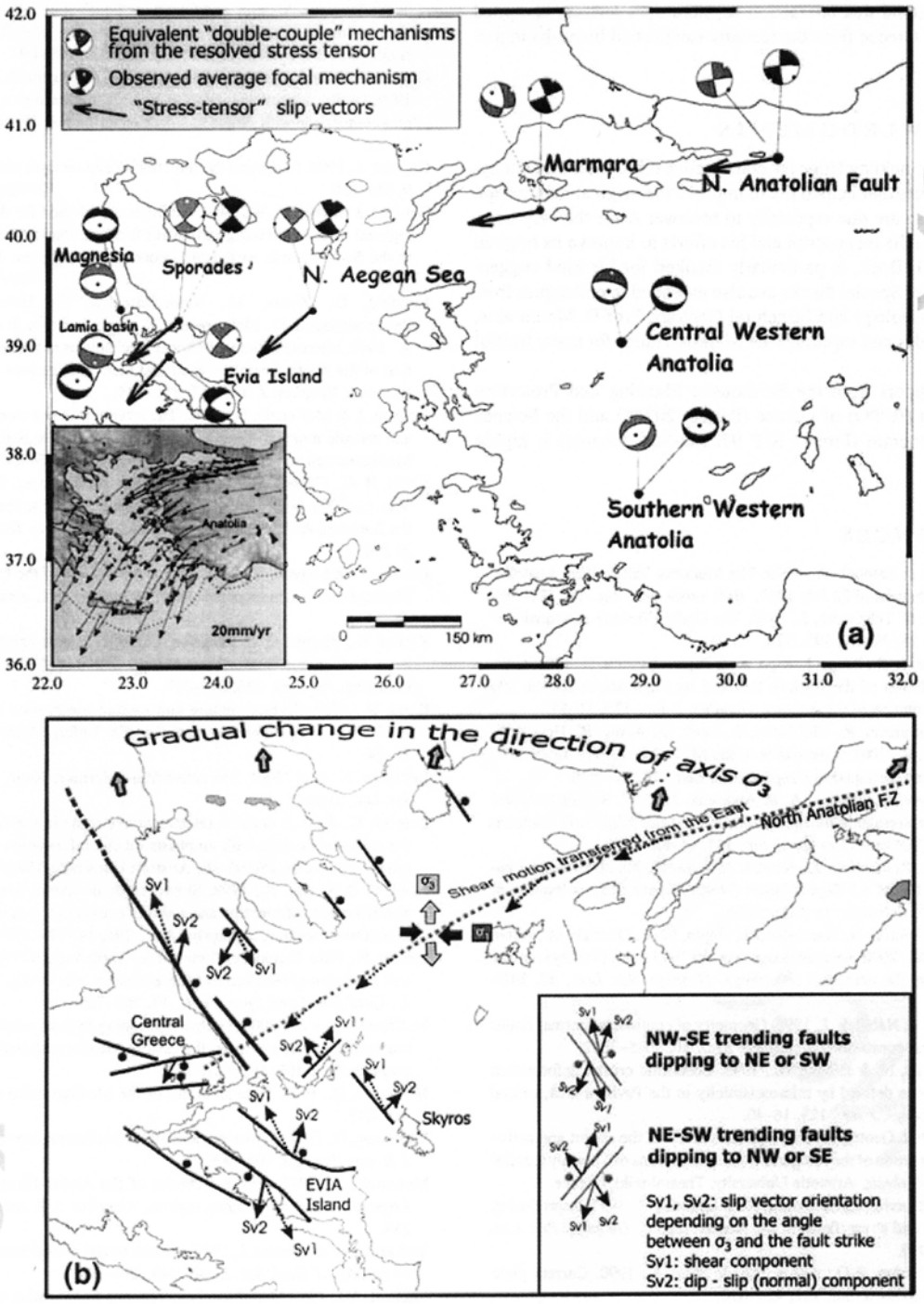

Figure 6. (a) Comparison of the double-couple mechanism corresponding to the regional stress tensor and of the average focal mechanism for each area. In most cases the agreement is very good indicating that the resolved stress tensors, obtained from the inversion of earthquake data at various scales, r eflect regional tectonics. Black arrows are slip vectors, corresponding to the 'stress tensor' mechanisms. The NE–SW trending planes connected with dextral strike-slip motion were taken as the fault planes along the NAF and its continuation in the N. Aegean Sea. The extrusion of the Anatolian plate towards the Aegean is clearly shown by the direction of these slip vectors which are in agreement with the GPS velocity vectors in a Eurasia fixed reference frame shown for comparison in the inset (data from McClusky *et al.* 2000). (b) A representation of the partition of shear motion in the NAF –central Greece interaction zone, showing the geometry of faults and the orientation of slip vectors (arrows). Depending on the fault strike in respect to the resolved σ_3 axis the normal or strike-slip component of motion is defined. Slip vectors associated with predominant normal components of motion are shown with straight lines whereas slip vectors associated with predominant strike-slip components of motion are shown with dashed lines.

NE–SW shear motion transferred. I believe in the future we will better understand this interaction as more data sets are compiled nowadays in Greece from the recently established broad-band networks.

ACKNOWLEDGMENTS

I would like to acknowledge the constructive criticism of two anonymous reviewers that helped me to improve the original manuscript. Special thanks are due especially to reviewer A for the very careful reading of the manuscript and his efforts to improve its original form. Prof G. Bock, is particularly thanked for his kind suggestions and help. Special thanks are also extended to colleagues from the Dept of Geology and Structural Geology, Prof D. Mountrakis, Prof S. Pavlides and especially Dr Markos Tranos for many fruitful discussions.

Partial support from the Earthquake Planning and Protection Organization (EPPO) of Greece (Project 20246) and the Science for Peace Program (Project SfP 972342/Seis-Albania) is highly appreciated.

REFERENCES

Ambraseys, N. & Zatopek, A., 1969. The Mudurnu Valley, West Anatolia, Turkey, earthquake of 22 July 1967, *Bull. seism. Soc. Am.*, **59,** 521–589.

Ambraseys, N. & Tchalenko, J., 1970. The Gediz (Turkey) earthquake of 1970 March 28, *Nature,* **227,** 592.

Armijo, R., Meyer, B., King, G., Rigo, A. & Papanastassiou, D., 1996. Quaternary evolution of the Corinth Rift and its implications for the late Cenozoic evolution of the Aegean, *Geophys. J. Int.*, **126,** 11–53.

Ayhan, M., Bürgmann, R., McClusky, S., Lenk, O., Aktug, B., Herece, E. & Reilinger, R., 2001. Kinematics of the M = 7.2, 12 November 1999, Düzce, Turkey earthquake, *Geophys. Res. Lett.*, **28,** 367–370.

Bellier, O., Over, S., Poisson, A. & Andrieux, J., 1997. Recent temporal change in the stress state and modern stress field along the North Anatolian Fault Zone (Turkey), *Geophys. J. Int.*, **131,** 61–86.

Benetatos, Ch., Roumelioti, Z., Kiratzi, A. & Melis, N., 2002. Source parameters of the M 6.5 Skyros Island (North Aegean Sea) earthquake of 2001 July 26, *Submitted for publication.*

Q4

Bouchon, M., Toks öz, N., Karabulut, H., Bouin, M.-P., Dietrich, M., Aktar, M. & Edie, M., 2000. Seismic imaging of the 1999 Izmit (Turkey) rupture inferred from the near-fault recordings, *Geophys. Res. Lett.*, **27,** 3013–3016.

Braunmiller, J. & Nábělek, J., 1996. Geometry of continental normal faults: Seismological constraints, *J. geophys. Res.*, **10,** 3045–3052.

Burton, P., Melis, N. & Brooks, M., 1995. Coseismic crustal deformation on a fault zone defined by microseismicity in the Pavliani area, central Greece, *Geophys. J. Int.*, **123,** 16–40.

Caputo, R., 1990. Geological and structural study of the recent and active brittle deformation of the Neogene-Quaternary basins of Thessaly (central Greece), *PhD thesis,* Aristotle University, Thessaloniki, Greece.

Cianetti, S., Gasperini, P., Boccaletti, M. & Giunchi, C., 1997. Reproducing the velocity and stress fields in the Aegean region, *Geophys. Res. Lett.*, **24,** 2087–2090.

DeMets, C., Gordon, R.G., Argus, D.F. & Stein, S., 1990. Current plate motions, *Geophys. J. Int.*, **101,** 424–478.

Dewey, J.F. & Seng ör, A.M.C., 1979. Aegean and surrounding regions: Complex multiplate and continuum mechanics in a convergence zone, *Geol. Soc. Am. Bull.*, **84,** 3137–3180.

Drakos, A., Stiros, S. & Kiratzi, A., 2001. Fault parameters of the 1980 (M_w = 6.5) Volos, central Greece, earthquake from inversion of repeated leveling data, *Bull. seism. Soc. Am.*, **91,** 1673–1684.

Engdahl, E., van der Hilst, R. & Buland, R., 1998. Global teleseismic earthquake relocation with improved travel times and procedures for depth determination, *Bull. seism. Soc. Am.*, **88,** 722–743.

Eyidoğan, H. & Jackson, J., 1985. A seismological study of normal faulting in the Demirci, Alasehir and Gediz earthquakes of 1969– 70 in western Turkey: Implications for the nature and geometry of deformation in the continental crust, *Geophys. J. R. astr. Soc.*, **81,** 569–607.

Gautier, P., Brun, J.-P., Moriceau, R., Soloutis, D., Martinod, J. & Jolivet, L., 1999. Timing, kinematics and cause of Aegean extension: a scenario based on a comparison with simple analogue experiments, *Tectonophysics,* **315,** 31–72.

Gephart, J., 1990. Stress and the direction of slip on fault planes, *Tectonics,* **9,** 845–858.

Gephart, J. & Forsyth, W., 1984. An improved method for determining the regional stress tensor using earthquake focal mechanism data: applications to the San Fernando earthquake sequence, *J. geophys. Res.*, **89,** 9305–9320.

Hatzfeld, D., Ziazia, M., Kemenzetzidou, D., Hatzidimitriou, P., Panagiotopoulos, D., Makropoulos, K., Papadimitriou, P. & Deschamps, A., 1999. Microseismicity and focal mechanisms at the western termination of the North Anatolian Fault and their implications for continental tectonics, *Geophys. J. Int.*, **137,** 891–908.

Jackson, J. & McKenzie, D., 1988. The relationship between plate motions and seismic moment tensors, and the rates of active deformation in the Mediterranean and Middle East, *Geophys. J.*, **93,** 45–73.

Kahle, H.-G., Cocard, M., Peter, Y., Geiger, A., Reilinger, R., Barka, A. & Veis, G., 2000. GPS-derived strain rate field within the boundary zones of the Eurasian, African, and Arabian plates, *J. geophys. Res.*, **105,** 23 353–23 370.

Kiratzi, A. & Louvari, E., 2001. Source parameters of the Izmit-Bolu 1999 (Turkey) earthquake sequences from teleseismic data, *Annali di Geofisica,* **44,** 33–47.

Kiratzi, A., Wagner, G. & Langston, C., 1991. Source parameters of some large earthquakes in Northern Aegean determined by body waveform modeling, *Pageoph,* **135,** 515–527.

Koral, H., 2000. Surface rupture and rupture mechanism of the October 1, 1995 (M = 6.2) Dinar earthquake, SW Turkey, *Tectonophysics,* **327,** 15–24.

LePichon, X. *et al.*, 2001. The active Main Marmara Fault, *Earthq. Planet. Sci. Let.*, in press.

Louvari, E., 2000. A detailed seismotectonic study in the Aegean Sea and the surrounding area with emphasis on the information obtained from microearthquakes, *PhD thesis,* Aristotle University, Thessaloniki, Greece.

Lund, B. & Slunga, R., 1999. Stress tensor inversion using detailed microearthquake information and stability constraints: Application to ölfus in southwest Iceland, *J. geophys. Res.*, **104,** 14 947–14 964.

Lyberis, N., 1984. Tectonic evolution of the North Aegean Trough, in *Geological Evolution of the Eastern Mediterranean,* eds Dixon, J. & Robertson, A., *Geol. Soc. Lond. Spec. Publ.*, **17,** 708–725.

McClusky, S. *et al.*, 2000. Global Positioning System constraints on plate kinematics and dynamics in the eastern Mediterranean and Caucasus, *J. geophys. Res.*, **105,** 5695–5720.

McKenzie, D., 1970. Plate tectonics of the Mediterranean region, *Nature,* 239–243.

McKenzie, D., 1972. Active tectonics of the Mediterranean region, *Geophys. J. R. astr. Soc.*, **30,** 109–185.

McKenzie, D., 1978. Active tectonics of the Alpine-Himalayan belt: the Aegean Sea and surrounding regions, *Geophys. J. R. astr. Soc.*, **55,** 217–254.

McKenzie, D. & Jackson, J., 1986. A block model of distributed deformation by faulting, *J. Geol. Soc. Lond.*, **143,** 249–253.

Michael, A.J., 1987. Use of focal mechanisms to determine stress: A control study, *J. geophys. Res.*, **92,** 357–368.

Nalbant, S., Hubert, A. & King, G., 1998. Stress coupling between earthquakes in northwestern Turkey and the north Aegean Sea, *J. geophys. Res.*, , **103,** 24 469–24 486.

Panagiotou, M., 2001. Seismic source parameters and fault-plane solutions of earthquakes in the north and central Aegean Sea, *MSc., thesis,* Aristotle University, Thessaloniki, Greece, p. 130.

Papazachos, C.B., 1999. Seismological and GPS evidence for the Aegean-Anatolia interaction, *Geophys. Res. Lett.*, **26,** 2653–2656.

Papazachos, B.C. & Papazachou, C., 1997. The Earthquakes of Greece, *Ziti Publications,* Thessaloniki, Greece, p. 304.

Papazachos, B., Panagiotopoulos, D., Tsapanos, T., Mountrakis, D. & Dimopoulos, G., 1983. A study of the 1980 summer seismic sequence in the Magnesia region of central Greece, *Geophys. J. R. astr. Soc.,* **75,** 155–168.

Papazachos, B., Kiratzi, A., Hatzidimitriou, P. & Karacostas, B., 1986. Seismotectonic properties of the Aegean area that restrict valid geodynamic models, "*Proc. 2nd WEGENER/MEDLAS conference,* May14–16, Athens, 1986," 1–16.

Papazachos, B., Kiratzi, A. & Papadimitriou, E., 1991. Regional Focal Mechanism for Earthquakes in the Aegean area, *Pure appl. Geophys.,* **136,** 407–420.

Papazachos, B., Papaioannou, Ch., Papazachos, C. & Savvaidis, A., 1997. Atlas of isoseismal maps for strong shallow earthquakes in Greece and surrounding area (426BC-1995), *Ziti Publications,* Thessaloniki, Greece, p. 176.

Papazachos, B.C., Papadimitriou, E.E., Kiratzi, A.A., Papazachos, C.B. & Louvari, E.K., 1998. Fault plane solutions in the Aegean Sea and the surrounding area and their tectonic implication, *Boll. Geof. Teor. App.,* **39,** 199–218.

Parker, R. & McNutt, M., 1980. Statistics for the one-norm misfit measure, *J. geophys. Res.,* **85,** 4429–4430.

Pavlides, S. & Tranos, M., 1991. Structural characteristics of two strong earthquakes in the North Aegean: Ierissos (1932) and Agios Efstratios (1968), *J. struct. Geol.,* **13,** 205–214.

Pavlides, S., Mountrakis, D., Kilias, A. & Tranos, M., 1990. The role of strike-slip movements in the extensional area of Northern Aegean (Greece), *Annales Tectonicae,* **IV,** 196–211.

Pinar, A., 1998. Source inversion of the October 1, 1995, Dinar earthquake (Ms = 6.1): a rupture model with implications for seismotectonics in SW Turkey, *Tectonophysics,* **292,** 255–266.

Pinar, A., Honkura, Y. & Kikuchi, M., 1996. A rupture model for the 1967 Mudurnu Valley, Turkey earthquake and its implication for seismotectonics in the western part of the North Anatolian Fault zone, *Geophys. Res. Lett.,* **23,** 29–32.

Ritsema, A., 1974. The earthquake mechanisms of the Balkan region, *R. Netherl. Meteorol. Inst., De Bilt, Sci. Rep.,* 74–4.

Rocca, A., Karakaisis, G., Karacostas, B., Kiratzi, A., Scordilis, E. & Papazachos, B., 1985. Further evidence on the strike slip faulting of the Northern Aegean trough based on properties of the August-November 1983 sequence, *"Bolletino di Geofisica Teorica ed Applicata ,"* **27,** 101–109.

Taymaz, T. & Price, S., 1992. The 1971 May 12 Burdur earthquake sequence, SW Turkey: a synthesis of seismological and geological observations, *Geophys. J. Int.,* **108,** 589–603.

Taymaz, T., Jackson, J. & McKenzie, D., 1991. Active tectonics of the north and central Aegean Sea, *Geophys. J. Int.,* **106,** 433–490.

Tibi, R. *et al.*, 2001. Rupture processes of the 1999 August 17 and November 12 Düzce (Turkey) earthquakes, *Geophys. J. Int.,* **144,** 1–7.

Tranos, M. & Mountrakis, D., 1998. Neotectonic joints of Northern Greece: their significance on the understanding of the active deformation, *Bull. Geol. Soc. Gr.,* **XXXII,** 209–219.

Wright, T.J., Parsons, B.E., Jackson, J.A., Haynes, M., Fielding, E.J., England, P.C. & Clarke, P.J., 1999. Source parameters of the 1 October 1995 Dinar (Turkey) earthquake from SAR interferometry and seismic bodywave modelling, *Earth planet. Sci. Lett.,* **172,** 23–37.

Wyss, M., Liang, B., Tanigawa, W. & Xiaoping, W., 1992. Comparison of orientations of stress and strain tensor based on fault-plane solutions in Kaoiki, Hawaii, *J. geophys. Res.,* **97,** 4769–4790.

Yagi, Y. & Kikuchi, M., 2000. Source rupture process of the Kocaeli, Turkey, earthquake of August 17, 1999, obtained by joint inversion of near-field data and teleseismic data, *Geophys. Res. Lett.,* **27,** 1969–1972.

Yilmazturk, A. & Burton, P., 1999. Earthquake source parameters as inferred from body waveform modelling, southern Turkey, *J. Geodyn.,* **27,** 469–499.

Zanchi, A. & Angelier, J., 1993. Seismotectonics of western Anatolia: regional stress orientation from geophysical and geological data, *Tectonophysics,* **222,** 259–274.

Zoback, M., 1992. First- and second-order patterns of stress in the lithosphere: The World Stress Map Project, *J. geophys. Res.,* **97,** 11 703–11 728.

AUTHOR QUERIES

Journal: GJI
Paper: gji1753

Dear Author

During the preparation of your manuscript for publication, the questions listed below have arisen. Please attend to these matters and return this form with your proof. Many thanks for your assistance.

Query Reference	Query	Remarks
1	Au:Please note it is GJI style to cite seismic events by year, month, day.	
2	Au:I added the link to the English Language version of the website. OK?	
3	Any update available?	
4	Au: Has this paper been accepted for publication yet? If so please provide update. If not please remove from reference list and cite as in prep. or pers comm. in the text	